

Paleoceanography and Paleoclimatology®



RESEARCH ARTICLE

10.1029/2025PA005194

Miocene Ocean Gyre Circulation and Gateway Transports— MioMIP1 Ocean Intercomparison

Key Points:

- Miocene gyres were weaker in Atlantic and South Pacific but stronger in North Pacific, likely due to wind stress and basin width change
- Miocene Antarctic Circumpolar Current was weaker than pre-industrial in 11 of 14 simulations
- Panama Seaway transport was westward in the early Miocene and gradually turned eastwards as Tethys Seaway shoaled and eventually closed

Supporting Information:

Supporting Information may be found in the online version of this article.

Correspondence to:

T. J. Naik,
trusha.naik@geo.su.se

Citation:

Naik, T. J., de Boer, A. M., Coxall, H. K., Burls, N. J., Bradshaw, C. D., Donnadieu, Y., et al. (2025). Miocene ocean gyre circulation and gateway transports—MioMIP1 ocean intercomparison. *Paleoceanography and Paleoclimatology*, 40, e2025PA005194. <https://doi.org/10.1029/2025PA005194>

Received 16 APR 2025













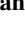




Accepted 5 NOV 2025

Author Contributions:

Conceptualization: Trusha J. Naik, Agatha M. de Boer, Helen K. Coxall
Data curation: Trusha J. Naik, Natalie J. Burls
Formal analysis: Trusha J. Naik
Funding acquisition: Agatha M. de Boer
Project administration: Agatha M. de Boer
Resources: Catherine D. Bradshaw, Yannick Donnadieu, Alexander Farnsworth, Amanda Frigola, Matthew Huber, Gregor Knorr, Allegra N. LeGrande, Yousheng Li, Gerrit Lohmann, Daniel J. Lunt, Matthias Prange
Software: Trusha J. Naik, Natalie J. Burls
Supervision: Agatha M. de Boer

© 2025. The Author(s).

This is an open access article under the terms of the [Creative Commons Attribution License](https://creativecommons.org/licenses/by/4.0/), which permits use, distribution and reproduction in any medium, provided the original work is properly cited.

Trusha J. Naik^{1,2} , Agatha M. de Boer^{1,2} , Helen K. Coxall^{1,2} , Natalie J. Burls³ , Catherine D. Bradshaw^{4,5} , Yannick Donnadieu⁶ , Alexander Farnsworth^{7,8} , Amanda Frigola^{9,10} , Matthew Huber¹¹ , Mehdi Pasha Karami¹² , Gregor Knorr¹³ , Allegra N. LeGrande^{14,15} , Yousheng Li⁷ , Gerrit Lohmann^{10,13} , Daniel J. Lunt⁷ , Matthias Prange¹⁰ , and Yurui Zhang¹⁶ 

¹Department of Geological Sciences, Stockholm University, Stockholm, Sweden, ²Bolin Centre for Climate Research, Stockholm, Sweden, ³Department of Atmospheric, Oceanic and Earth Sciences, Center for Ocean-Land Atmosphere Studies, George Mason University, Fairfax, VA, USA, ⁴The Global Systems Institute, University of Exeter, Exeter, UK, ⁵Met Office Hadley Centre, Exeter, UK, ⁶Aix Marseille University, CNRS, IRD, Coll France, INRA, CEREGE, Aix en Provence, France, ⁷School of Geographical Sciences, University of Bristol, Bristol, UK, ⁸Tibetan Plateau Earth System, Environment and Resources (TPESER), Institute of Tibetan Plateau Research, Chinese Academy of Sciences, Beijing, China, ⁹Barcelona Supercomputing Center, Barcelona, Spain, ¹⁰MARUM – Center for Marine Environmental Sciences, University of Bremen, Bremen, Germany, ¹¹Department of Earth, Atmospheric, and Planetary Sciences, Purdue University, West Lafayette, IN, USA, ¹²Rosby Centre, Swedish Meteorological and Hydrological Institute, Norrköping, Sweden, ¹³Alfred Wegener Institute Helmholtz Centre for Polar and Marine Research, Bremerhaven, Germany, ¹⁴NASA Goddard Institute for Space Studies, New York, NY, USA, ¹⁵Center for Climate Systems Research, Columbia University, New York, NY, USA, ¹⁶State Key Laboratory of Marine Environmental Science, College of Ocean & Earth Sciences, Xiamen University, Xiamen, China

Abstract The Miocene (~23–5 Ma) experienced substantial paleogeographic changes, including the shoaling of the Panama Seaway and closure of the Tethys Seaway, which altered exchange pathways between the Pacific and Atlantic Oceans. Changes in continental configuration and topography likely also influenced global wind patterns. Here, we investigate how these changes affected surface wind-driven gyre circulation and interbasin volume transport using 14 fully coupled climate model simulations of the early and middle Miocene. The North and South Atlantic gyres, along with the South Pacific gyre, are weaker in the Miocene simulations compared to pre-industrial (PI), while the North Pacific gyres are stronger. These changes largely follow the wind stress curl and basin width changes. Westward flow through the Panama Seaway occurs only in early Miocene simulations when the Tethys Seaway is open and transports are strongly westward. As the Tethys transport declines, flow across the Panama Seaway gradually reverses from westward (into the Pacific) to eastward (into the Atlantic). In simulations with a closed Tethys Seaway, the Panama transport is consistently eastward. The Southern Hemisphere westerlies are weaker than PI in all simulations, contributing to a reduced Antarctic Circumpolar Current (ACC) in 11 of the 14 cases. In the remaining three, a stronger ACC is simulated, likely due to a combination of enhanced meridional density gradients and model-dependent sensitivities. These findings highlight how changes in Miocene seaways and wind patterns reshaped ocean circulation, influencing interbasin exchange, thermohaline properties, and global climate.

Plain Language Summary The Miocene (~23–5 million years ago) experienced major paleogeographic changes, such as shoaling of ocean gateways and shifts in topography and continental positions. These changes likely influenced how water was exchanged between ocean basins. Here, we use 14 atmosphere-ocean climate model simulations of the early and middle Miocene (~12–20 million years ago) to investigate their impact on ocean circulation. We find that wind-driven gyres were weaker in the Atlantic and South Pacific, but stronger in the North Pacific compared to today. These patterns closely follow changes in wind stress and basin width. The direction of flow through the Panama Seaway, which once connected the Atlantic and Pacific, was linked to the transport through the Tethys Seaway. When the Tethys Seaway was open, flow through the Panama Seaway could be westward, but once it closed, the flow reversed eastward into the Atlantic. In the Southern Ocean, weaker winds led to a weaker Antarctic Circumpolar Current (ACC) in most simulations. However, in a few cases, a stronger ACC emerged, likely due to enhanced density gradients and differences in model physics. Together, these results highlight how Miocene seaway and wind changes reshaped global ocean circulation and climate.

Visualization: Trusha J. Naik

Writing – original draft: Trusha J. Naik, Agatha M. de Boer

Writing – review & editing: Trusha J. Naik, Agatha M. de Boer, Helen K. Coxall, Natalie J. Burls, Catherine D. Bradshaw, Yannick Donnadieu, Alexander Farnsworth, Amanda Frigola, Matthew Huber, Mehdi Pasha Karami, Gregor Knorr, Allegra N. LeGrande, Yousheng Li, Gerrit Lohmann, Daniel J. Lunt, Matthias Prange, Yurui Zhang

1. Introduction

The horizontal circulation of the ocean consists of the wind-driven gyres in the upper ocean, the interbasin transport through oceanic gateways and the horizontal component of the thermohaline circulation. This circulation redistributes momentum and energy and transports tracers such as salinity, nutrients, and dissolved gases within basins and between them via gateways such as the Bering Strait. The gyres themselves are composed of stronger subtropical anti-cyclonic gyres and weaker subpolar cyclonic gyres.

The structure and variability of wind-driven gyre circulation play a key role in modulating oceanic heat transport and deep overturning circulation in the modern ocean. In the North Pacific, this gyre circulation dominates oceanic heat transport, carrying the majority of the total transport northwards (Ferrari & Ferreira, 2011). In contrast, the North Atlantic contributes a smaller but still substantial share (up to ~40%) to poleward heat transport, which remains climatically significant and influences variability on seasonal to millennial timescales (Ferrari & Ferreira, 2011; Palter, 2015; Talley, 2003). Variability in the North Atlantic Subpolar Gyre (SPG), which is driven by changes in wind stress and heat fluxes, has also been linked to shifts in the Atlantic Meridional Overturning Circulation (AMOC) (Böning et al., 2006).

The strength and structure of gyres across basins are influenced by the curl of wind stress (Munk, 1950). For example, in the modern ocean, changes in wind stress have been shown to affect the strength and position of gyres in both the Pacific and Atlantic, although the response can differ between the two basins depending on regional atmospheric forcing. These effects are evident in present-day observations (Drouin et al., 2021), future projections (Yang et al., 2020) and reconstructions of past climates (Gray et al., 2020; Xing et al., 2022; Zhang et al., 2020, 2025).

Earlier in the Cenozoic, paleogeography and climate were different, resulting in different ocean and atmospheric conditions. Under greenhouse warmth of the Eocene (~56–34 Ma), when Australia and Africa were situated further south, closer to Antarctica, and the Pacific was significantly larger than today, models suggest that wind stress and gyre circulation were different, and produced more hemispherically symmetrical zonal winds around the equator than today, stronger gyres in the Pacific and weaker gyres in the Atlantic (Zhang et al., 2020). The transports through the straits were also different, with the Antarctic Circumpolar Current (ACC) being absent in the early Eocene due to the highly restricted Drake Passage and Tasmanian Gateway (Sarkar et al., 2019; Toumoulin et al., 2020; Zhang et al., 2020, 2025). The Miocene (~23–5 Ma) lies between the Eocene and the modern day in terms of paleogeography and climate (Straume et al., 2020; Westerhold et al., 2020). During the Miocene, the global climate was substantially warmer, comparable to projected future warming under high emissions, and the paleogeography was different compared to the modern configuration, with open tropical oceanic gateways and differences in elevation of mountain range (Steinhorsdottir et al., 2021). While some studies have investigated the importance of the opening or closing of individual gateways on ocean circulation and climate during the Miocene, the general impact of the Miocene paleogeography on the gyres and strait flows is not well known (e.g., Hossain et al., 2021; Pillot et al., 2022; von der Heydt & Dijkstra, 2006).

Arguably, the most striking gateway changes during the Miocene were the narrowing and restriction of the tropical gateways. During the early Miocene (~23–16 Ma), the Panama Seaway was open and deep and it started shoaling during the middle Miocene (~16–12 Ma) (Kirillova et al., 2019) and may have reached a critical depth between 50 and 200 m by ~10 Ma (Sepulchre et al., 2014). However, some studies suggest that the Panama Seaway was already too shallow for deepwater exchange by the middle Miocene, and only intermittent shallow water settings in the region occurred subsequently (Montes et al., 2012, 2015; Ramírez et al., 2016). The Tethys Seaway, which connected the Mediterranean Sea to the Indian Ocean, started closing in the early Miocene ~20 Ma, and closed completely by ~13 Ma (Bialik et al., 2019). The Indo-Australian plate had moved much further north by the Miocene compared to the Eocene, resulting in the narrowing of the Indonesian Seaway, after which it was possibly no longer a deep-water pathway between the Indian and Pacific oceans (Gallagher et al., 2024; Kuhnt et al., 2004). Changes in these gateway configurations during the Miocene likely resulted in an interplay between the volume transport (VT) across them.

The role of the Panama Seaway oceanic exchange on AMOC has been debated for more than a decade (Brierley & Fedorov, 2016; Krapp & Jungclauss, 2011; Lunt et al., 2008). However, the majority of studies suggest that the shallowing and subsequent closure of the Panama Seaway during the Miocene and the Pliocene (~5.3–2.6 Ma) was important for either initiating or strengthening the overturning circulation in the Atlantic, paving the way for

an Atlantic-dominated global overturning (Lunt et al., 2008; Schneider & Schmittner, 2006; Zhang et al., 2012; Ögretmen et al., 2020). The closure of the Eastern Tethys Seaway blocked the water from the Indian Ocean from reaching the North Atlantic (Karami, 2011). This could have contributed to the intensification of the deep-water formation in the North Atlantic, through warming and changes in sea surface salinity and reversal of flow through the Panama Seaway (von der Heydt & Dijkstra, 2005; Zhang et al., 2011). Thus, the oceanic gateways exert control over the overturning circulation and affect the freshwater and heat advection (Ögretmen et al., 2020) by restricting the VT between basins.

Several studies link the transport through the Panama Seaway to the wind stress, using the “island rule” (Godfrey, 1989). The island rule is derived by integrating the linear momentum equations around an island, which results in an expression where the upper circulation above a level of no motion around the island is given by the integral of the wind stress along a closed path (Text S1 in Supporting Information S1). Using the island rule Omata and Dijkstra (2003) showed that when the transport through Tethys Seaway reduced, and the transport through the Drake Passage increased enough, the Panama Seaway transport switched from westward (into the Pacific) to eastward (into the Atlantic). Nof and Van Gorder (2003), applied the island rule to numerical simulations with a reduced gravity 1½-layer model, with different configurations of open and closed Bering and Panama Seaways and an active and inactive North Atlantic Deep Water (NADW) formation. They reported that an intrusion of Pacific waters into the Atlantic via the Panama Seaway is only possible if there is a reduced rate of NADW formation.

Furthermore, some of the high-latitude gateways were opening/widening throughout the Miocene, which may also have significantly altered the ocean circulation and climate. The Fram Strait was shallow until the late early Miocene (~17–18 Ma) and it has been proposed that the freshwater flow through it was unidirectional (Arctic to North Atlantic) and controlled hydraulically, after which it deepened and widened allowing a bi-directional flow (Ehlers & Jokat, 2013; Hossain et al., 2020, 2021; Jakobsson et al., 2007). The Greenland-Scotland Ridge (GSR) likely deepened in two stages, during the early and middle Miocene, which increased the overflow of dense waters in the North Atlantic, likely strengthening the overturning circulation (Uenzelmann-Neben & Gruetzner, 2018). The Drake Passage opened before the Miocene, likely in the Eocene, although the exact timing remains poorly constrained, with the timing of the opening of the passage ranging from the early Eocene ~50 Ma (van de Lagemaat et al., 2021) to the middle Eocene ~41 Ma (Scher & Martin, 2006) and as late as the Oligocene ~31–26 Ma (Hodel et al., 2021). Evidence from stratigraphic records suggests that tectonic uplift led to a constriction of the passage from ~26 to 14 Ma, which may have caused a temporary weakening of the ACC (Lagabriele et al., 2009). After 14 Ma, the Drake Passage widened, and the ACC strengthened again. The Pacific-Arctic connection through the Bering Strait was closed throughout most of the Miocene, perhaps opening up during the late Miocene, leaving the Fram Strait as the only connection to the Arctic for most of the Miocene (Gladenkov, 2004; Hall et al., 2023).

While several studies have explored the effects of individual gateway changes on circulation, the broader impacts of Miocene paleogeography on the strength and structure of the gyres and volume transports remain poorly understood. In particular, it is unclear how the combination of different wind stress patterns, gateway configurations, and continental positions influenced the large-scale horizontal circulation during this time. The extent to which the Miocene gyre system had transitioned toward a modern-like structure, with distinct subtropical and subpolar gyres in both the northern and southern basins of the Atlantic and Pacific, and how these changes may have shaped interbasin exchange and ACC variability, also remain open questions. Here, we make opportunistic use of the MioMIP1 ensemble (Burls et al., 2021) which consists of 14 fully coupled climate model simulations of the early and middle Miocene. With these, we investigate the Miocene horizontal circulation in a set of simulations that sample a wide range of boundary conditions in different models and attempt to bridge the gaps mentioned above. In Section 2, we describe the models and methods used in this study. The gyres are described using the barotropic streamfunctions in Section 3, followed by an investigation of the volume transports through the different straits and their interdependence in Section 4. Finally, in Section 5, we provide a summary and the conclusions of this study.

2. Models and Methods

2.1. Models

We use 14 simulations in this study, carried out with 7 fully coupled Earth System Models simulating the Miocene using a range of boundary conditions (Table 1). The details of the simulations used are provided in Burls et al. (2021), the published studies from which they originated (Table 1), as well as Naik, Boer, Coxall, et al. (2025). Table 1 briefly summarizes this information for the early and middle Miocene simulations used in this study.

2.2. Wind Stress Curl and Sverdrup Transport

Wind blowing over the ocean surface exerts a force that transfers momentum from the atmosphere to the upper ocean. This force is referred to as wind stress (τ), with the zonal and meridional components denoted by τ_x and τ_y , respectively. Because the wind field varies spatially, it produces gradients in wind stress. The wind stress curl, which represents the rotational component of this forcing, is defined as:

$$\text{Curl}(\tau) = \frac{\partial \tau_y}{\partial x} - \frac{\partial \tau_x}{\partial y} \quad (1)$$

Sverdrup (1947) demonstrated that, away from the western boundary currents, a negative wind stress curl causes convergence and downwelling in the water column, resulting in an equatorward Sverdrup transport, as seen in subtropical gyres. Conversely, a positive wind stress curl leads to divergence and upwelling, producing a poleward Sverdrup transport characteristic of subpolar gyres (Thomas et al., 2014). This relationship, known as the Sverdrup balance, is expressed as:

$$\beta V_{Sv} = \frac{1}{\rho} \left(\frac{\partial \tau_y}{\partial x} - \frac{\partial \tau_x}{\partial y} \right) \quad (2)$$

where, $\beta = \frac{df}{dy}$ is the rate of change of the Coriolis parameter f with latitude, V_{Sv} is the volume transport arising due to Sverdrup balance and ρ is the density of seawater. In this study, we use only the meridional gradient of the zonal wind stress term ($\frac{\partial \tau_x}{\partial y}$) as a simplified representation of the curl, since this term generally dominates and captures the primary wind-driven control on gyre circulation.

2.3. Barotropic Streamfunction

The barotropic streamfunction (BSF) describes the horizontal flow, integrated from the north to south and vertically to the full depth, reflecting the total horizontal transport of water through the entire depth. It captures the important features of the Sverdrup transport, such as the wind-driven gyres and currents (Huber et al., 2004). The BSF is available as a model output for all but two simulations from the IPSLCM5 model. It is calculated as,

$$\Psi(x, y) = \int_{y_N}^y \int_{-H}^0 u(x, y', z) dz dy' \quad (3)$$

where $u(x, y', z)$ is the zonal velocity integrated from the north y_N to y and from the sea surface to the bottom $-H$. The red (positive) contours indicate a clockwise (anti-cyclonic) circulation, and the blue (negative) contours show an anti-clockwise (cyclonic) circulation. The latitudinal strength of the gyre transport is defined as the maximum magnitude of transport at that latitude. If the magnitude of the negative transport exceeds that of the positive transport, the maximum value is taken as negative.

3. Barotropic Streamfunction and Gyre Transports

The global wind pattern over the ocean surface drives divergent flow in the surface Ekman layer, that induces downwelling in the subtropics and upwelling in the equatorial and subpolar regions. To balance the change in potential vorticity from this stretching and squeezing of the water column, the fluid must move meridionally to a different background planetary vorticity. The meridional transport, referred to as Sverdrup transport, can be

Table 1
Configuration and Key Settings of Each Simulation Used in This Study

Model	Resolution (Atm/Ocn)	Length (Years analyzed)	CO ₂ (ppm)	Paleogeography	Ice sheets	Target time period	Depth of gateways (m)	Reference
CCSM3_F	T42–2.8°/1°	1,500 (last 100)	400	Frigola et al. (2018)	No GIS, AIS ~ 18 m SLE	16.7–14.5 Ma	PS: 514 TS: 814 DP: 3,750	Frigola et al. (2018)
CCSM3_H	T31–3.75°/~3° × 1.5°	1,100 (last 100)	355	Herold et al. (2011)	Herold et al. (2008); AIS height reduced by 1,000 m	20–14 Ma	PS: 3,030 TS: 686 DP: 3,516	Herold et al. (2011)
CCSM4	~1.9° × 2.5°/1°	2,000 (last 100)	400	Herold et al. (2011) (updated)	GIS ~ 0.87 m SLE, AIS ~ 19.6 m SLE	20–14 Ma	PS: 3,751 TS: 120 DP: 3,503	Burlis et al. (2021)
CESM1	~1.9° × 2.5°/1°	3,000 (last 50)	400	Herold et al. (2011) (updated)	GIS ~ 0.87 m SLE, AIS ~ 19.6 m SLE	20–14 Ma	PS: 3,751 TS: 120 DP: 3,503	Burlis et al. (2021)
IPSLCM5	3.75° × 1.875°/2°–0.5°	3,000 (last 100)	560	Poblete et al. (2021)	AIS, no GIS, Tethys 120 m	20 Ma	PS: 1,033 TS: 0 DP: 3,752	Pillot et al. (2022)
IPSLCM5_T			560		AIS, no GIS, Tethys closed	20 Ma	PS: 1,033 TS: 120 DP: 3,752	
HadCM3L_B1	3.75° × 2.5°/3.75° × 2.5°	2,000 (last 50)	400	Markwick (2007)	No GIS, No AIS	15.9–11.6 Ma	PS: 995 TS: 0 DP: 2,731	Bradshaw et al. (2021)
HadCM3L_B2			400		No GIS, AIS - 55 m SLE			
HadCM3L_F1	3.75° × 2.5°/3.75° × 2.5°	7,422 (last 100)	400	Getech Plc.	AIS, No GIS	15.9–13.8 Ma	PS: 995 TS: 0 DP: 2,116	Farnsworth et al. (2019)
HadCM3L_F2			760			15.9–13.8 Ma		
HadCM3L_F3			400			13.8–11.6 Ma	PS: 995 TS: 0 DP: 2,116	
HadCM3L_L1			494	Scotese and Wright (2018)		15.9–13.8 Ma	PS: 2,731 TS: 0 DP: 2,731	Judd et al. (2024)
COSMOS	3.75° × 3.75°/~3°	2,000 (last 100)	450	Herold et al. (2011) + NA/Arctic reconstruction (Ehlers & Jokat, 2013)	No GIS, AIS - Herold et al. (2008)	20–14 Ma	PS: 3,395 TS: 740 DP: 3,395	Stärz et al. (2017)
GISS	2° × 2.5°/1° × 1.25°	5,000 (last 100)	456	Frigola et al. (2018)	No GIS, AIS ~ 18.1 m SLE	16.7–14.5 Ma	PS: 1,214 TS: 745 DP: 3,565	Naik, Boer, Coxall, et al. (2025)

Note. AIS—Antarctic Ice Sheet; GIS—Greenland Ice Sheet; SLE—Sea Level rise Equivalent - defined as the amount of sea level rise (in meters) that will occur if the ice-sheet melts completely. A smaller ice sheet SLE value means a smaller ice sheet and vice versa, with the modern AIS size ≈58 m SLE (Pritchard et al., 2025) and modern GIS ≈ 7.4 m SLE (Mortlighem et al., 2017); PS—Panama Seaway; TS—Tethys Seaway; DP—Drake Passage.

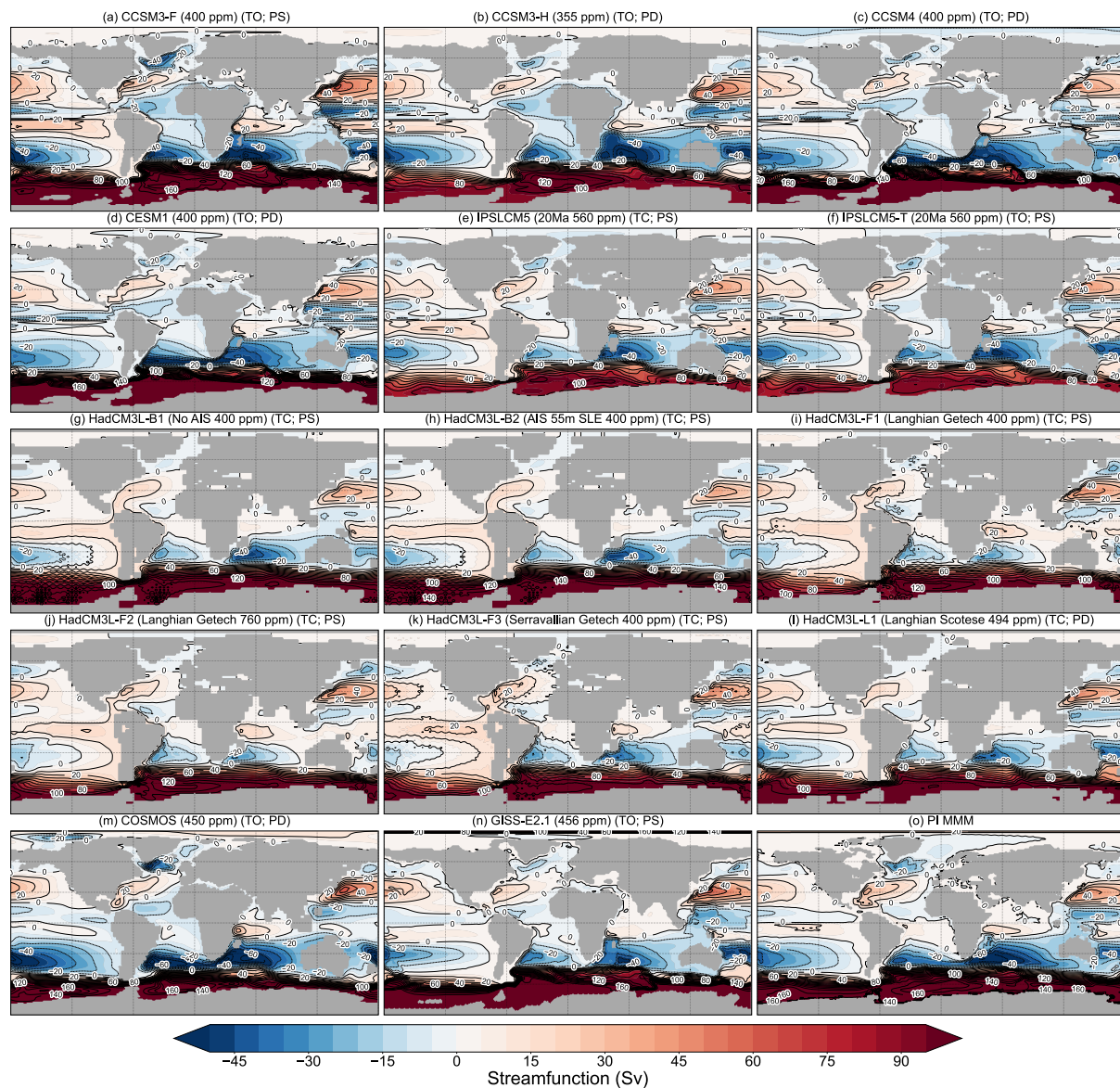


Figure 1. Barotropic streamfunction for the Miocene simulations. These simulations are part of an opportunistic multi-model intercomparison, using slightly different model setups that approximate early to middle Miocene conditions (see Table 1 for details on paleogeography and boundary conditions). Red contours (positive) indicate anticyclonic circulation and blue contours (negative) indicate cyclonic circulation. The final panel (o) is the multi-model mean (MMM) of the pre-industrial (PI) simulations. Panel labels (a–n) list the simulation name, the atmospheric CO₂ concentrations, and, where needed, additional descriptors that distinguish simulations with similar names (e.g., paleogeographies used, Antarctic Ice Sheet size, etc.). Abbreviations in the panel titles denote whether the Tethys Seaway is open or closed and Panama Seaway is shallow (<1,500 m) or deep (>1,500 m); TO—Tethys open, TC—Tethys closed, PS—Panama shallow, PD—Panama deep.

related directly to the curl of the wind stress, in what is known as the “Sverdrup balance” (Sverdrup, 1947; Equation 2). The Sverdrup transport arising due to this balance is equatorward in the subtropics and poleward in the subpolar regions. The interior Sverdrup transport is returned in the western boundary current where bottom drag and eddy viscosity become important in the vorticity balance, essentially closing the gyre circulation (Munk, 1950; Stommel, 1948). The maximum strength of the gyre circulation is the zonal integration of the meridional Sverdrup transport and is set by the width of the basin and the strength of the wind stress curl. Although this theory does not work in the high latitudes and western boundary regions, it holds fairly well in the interior subtropical oceans (Aoki & Kutsuwada, 2008; De Boer et al., 2013; Thomas et al., 2014). Thus, we can expect wind stress curl to play an important role in setting the gyre strength in this region. Here, we study the gyres in our simulations using the BSF (Figure 1, Equation 3).

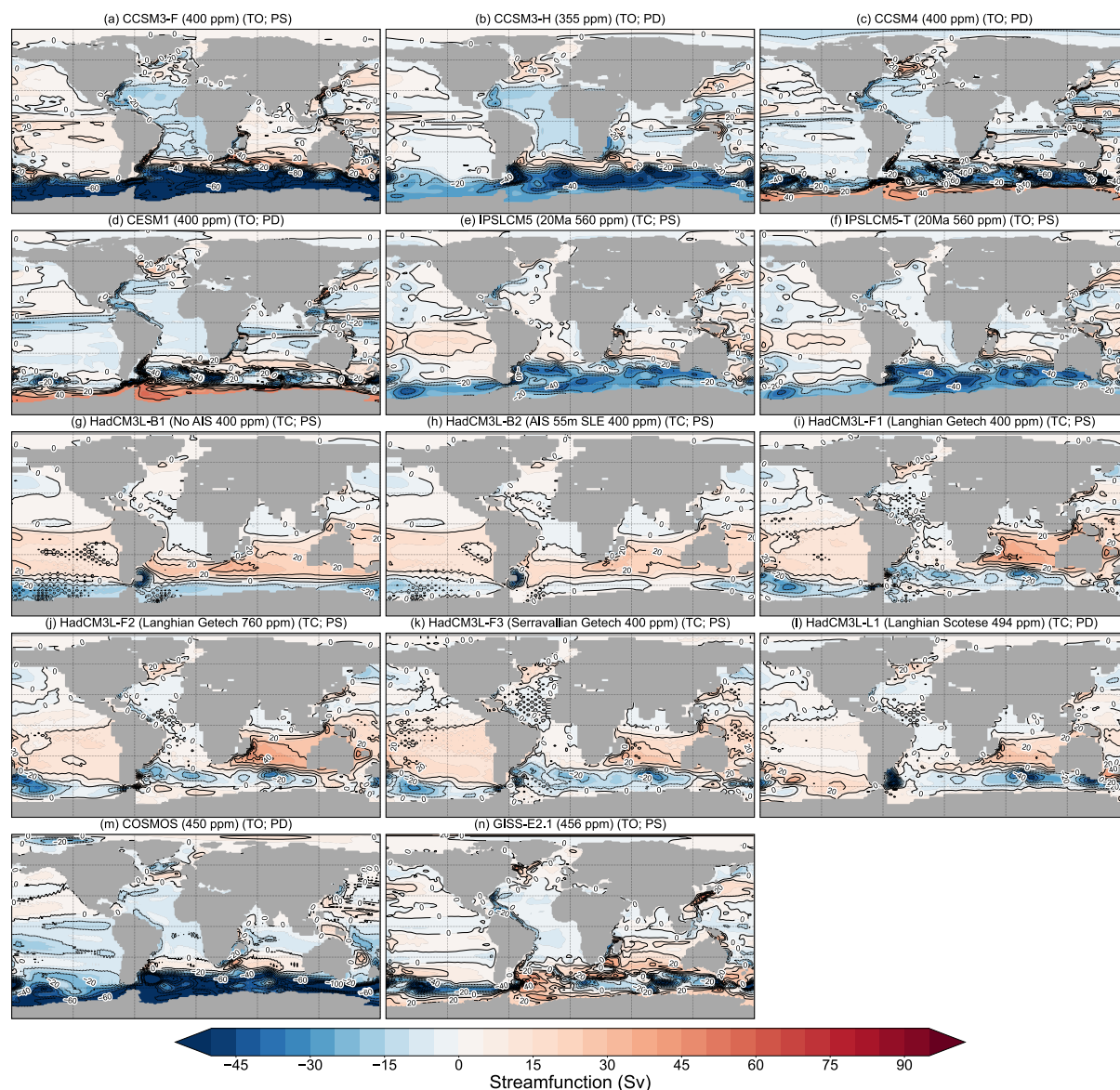


Figure 2. The difference between Miocene and PI barotropic streamfunction (Miocene-PI). A weakening of the positive contours in the Miocene simulations will show up as negative values (blue contours) while a weakening of negative contours will show up as positive values (red contours). Panel labels and abbreviations denote the same as in Figure 1.

The open Panama Seaway in the Miocene simulations leads to obvious differences in the vertically integrated barotropic streamfunctions in the Atlantic during the Miocene (Figure 1) compared to the pre-industrial simulations (Figure S1 in Supporting Information S1). It permits a low-latitude exchange between the Atlantic and Pacific, leading the streamlines to cross the seaway. The most prominent features are the subtropical gyres and comparatively weaker subpolar gyres in all the ocean basins during the Miocene, which overall look like the modern gyre pattern (Figure 1). The spatial difference between the Miocene and PI simulations (Figure 2) shows that the Gulf Stream along the east coast of North America is weaker during the Miocene, where the negative values indicate a weakening compared to the PI. The SPG region in the North Atlantic exhibits positive values in most simulations in Figure 2, indicating a weakening during the Miocene, since the SPG contours are negative. Two simulations, COSMOS and CCSM3_F, show a stronger SPG during the Miocene as shown by the negative contours (Figure 2).

The strength of gyre transport and average zonal wind stress in the Atlantic for individual simulations are shown in Figures S2 and S3 in Supporting Information S1, respectively, and for the Pacific in Figures S4 and S5 in Supporting Information S1, respectively. The simulations exhibit a wide intermodel spread in gyre strength, likely due to differences in wind fields and paleogeographies (Figures S2 and S4 in Supporting Information S1). However, the direction of change between the Miocene and PI simulations is consistent across most models, where a majority of simulations show weaker Miocene gyres in the North and South Atlantic and the South Pacific, and stronger Miocene gyres in the North Pacific compared to PI (Tables S1a and S1b in Supporting Information S1). Even though the Miocene simulations differ locally in gateway depths and orography, the overall changes relative to PI are generally the same (e.g., a closed Panama Seaway in PI vs. an open Panama Seaway in the Miocene). We therefore use the multi-model mean (MMM) to highlight trends in gyre transport, noting that the MMM also reflects the tendency found in most models. The MMM is somewhat biased by the fact that different models run on different paleorotational reference frames. However, this impact is likely small, especially in the ocean interiors, and the MMM approach has previously been applied, for example, to the Eocene (Lunt et al., 2012), for which the reference frame differences are even larger than here.

The MMM strength of the gyres for both the Miocene and PI indicates that the Atlantic gyres were weaker in both the northern and southern basins (Figure 3a). North Atlantic SPG is 35% weaker, the STG is 28% weaker, and the South Atlantic STG is 9% weaker in the Miocene simulations (Table S1a in Supporting Information S1). The weaker gyres may be the result of the weaker MMM zonal average wind stress in the Miocene compared to PI, with reductions in peak tropical easterlies, subtropical westerlies, and northern hemisphere polar easterlies (Figure 3c). The reduced winds translate into a weaker meridional gradient of zonal wind stress ($d\tau_x/dy$) in the Miocene simulations which affects the gyre strength through the Sverdrup balance (Figures 3d, Equation 2). Another factor that may explain the weaker Miocene gyres, is the generally smaller width of the Atlantic basin (Figure 3b). Indeed, an estimate of the Sverdrup transport where the meridional gradient of the zonal wind stress is multiplied by the basin width (see Section 2.2), illustrates a more pronounced weakening of the gyres during the Miocene than from the wind stress gradient alone (Figure 3e), indicating that both the basin width and the winds play a role in the weaker gyres seen in Figure 3a.

In the North Pacific, the MMM of the gyre strength indicates that both the STG and the SPG are similar to PI strength in the Miocene (Figure 3f; cf. Eocene Pacific gyres in Zhang et al., 2025). However, the percentage change in gyre strength for individual simulations reveals that the North Pacific gyres, especially the SPG, are stronger in the Miocene compared to PI (Table S1b in Supporting Information S1), where the SPG is 84% stronger and the STG is 13% stronger in the Miocene. This indicates that although the overall direction of change (stronger Miocene gyres) is consistent across most models, the large intermodel spread, particularly in the SPG, reduces the signal in the MMM, making the mean appear close to PI strength. This strengthening is likely due to a combination of slightly stronger wind stress curl and a wider Miocene North Pacific basin (Figures 3g, 3i and 3j). The spatial difference between the Miocene and PI reveals a distinct strengthening of the western boundary current in the Miocene, called the Kuroshio current, indicated by the positive (red) contours in the western subtropical North Pacific (Figure 2). The South Pacific STG is weaker in the Miocene than in the PI (Figure 3f), likely due to a weaker Miocene wind stress curl amplitude along the gyre latitudes (Figure 3i), which would have reduced Ekman pumping and the associated subtropical recirculation that sustains the gyre.

4. Circulation Through Straits

In this opportunistic model intercomparison, since the models use different paleogeographies (see Section 2.1), the geometries of the straits, including depth, latitude, and width, are different in all the simulations. We have previously analyzed the impact of zonal VT through the Panama Seaway and Tethys Seaway on the AMOC and PMOC in Naik, Boer, Coxall, et al. (2025), which explores the factors influencing the meridional overturning circulation. Here, we examine the controls of the gateway transports themselves, and how the volume transports of the tropical gateways relate to each other. We only look at the zonal VT across the gateways. The values of the zonal VT through all the straits are given in Table 2. We also examine the cross-sections and depth of the straits and seaways that played a role in controlling the large-scale circulation during the Miocene. For the Panama Seaway, we compare the depth of the seaway against the zonal VT as there are estimations available for the depth of the gateway during the Miocene (Sepulchre et al., 2014). The size of the cross-sections indicates which time periods the simulation best represents (i.e., where in the paleogeographic evolution it fits). It is often assumed that with a shoaling of the Panama Seaway, the Pacific-Atlantic throughflow is reduced (Newkirk & Martin, 2009).

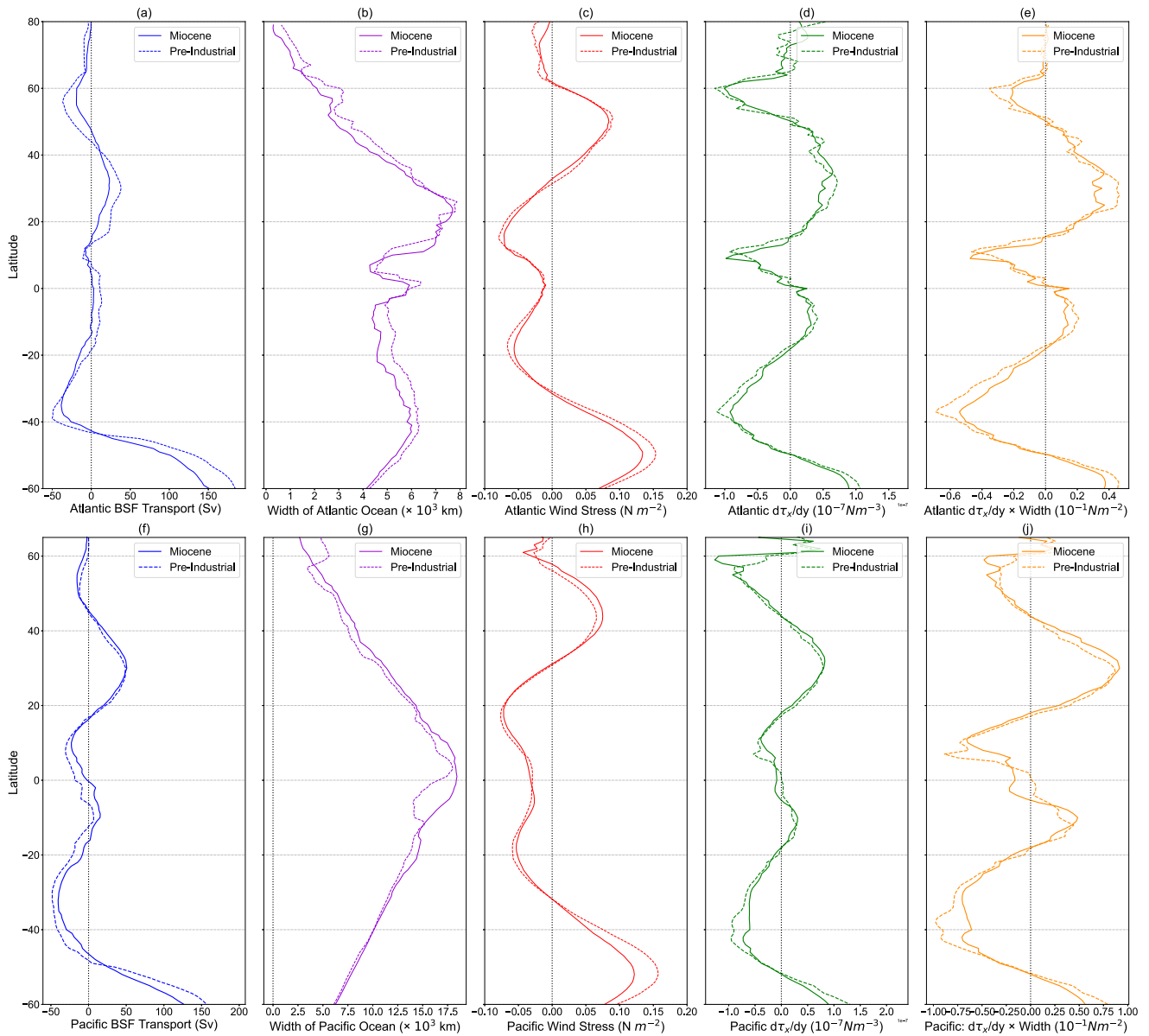


Figure 3. (a) The multi-model mean (MMM) strength of gyre transport (BSF transport; Sv) in the Atlantic Ocean. The strength of the gyres is the zonal maximum magnitude of transport in the basin, and if the maximum transport is negative, the maximum value is taken as negative. (b) The MMM width of the Atlantic basin (km). (c) MMM average zonal wind stress (τ_x) over the Atlantic Ocean (Nm^{-2}). (d) Meridional gradient of the MMM zonal average wind stress ($d\tau_x/dy$; Nm^{-3}) over the Atlantic Ocean. (e) Atlantic $d\tau_x/dy \times$ Atlantic width (Nm^{-2}). (f) MMM strength of gyre transport in the Pacific Ocean (Sv). (g) MMM width of the Pacific basin (km). (h) MMM average zonal wind stress (τ_x) over the Pacific Ocean (Nm^{-2}). (i) Meridional gradient of the MMM zonal average wind stress ($d\tau_x/dy$; Nm^{-3}) over the Pacific Ocean. (j) Pacific $d\tau_x/dy \times$ Pacific width (Nm^{-2}). The solid lines are Miocene values, and the dashed lines are the PI values.

However, that might only be true when the strait depth or section reaches a critical level, after which its flow is frictionally restricted by form drag. Here, we test the extent to which the volume transport is controlled by the cross-section or depth of the seaway and whether the volume transport through a strait increases monotonically with the cross-section of the strait.

We start with the tropical gateways, the Panama and Tethys Seaways, which experienced major changes throughout the Miocene. Closure of these gateways in the Neogene led to the cessation of low-latitude water mass exchange between the Atlantic, Pacific, and Indian Oceans (Bialik et al., 2019; Kirillova et al., 2019). We also briefly mention the Indonesian Throughflow (ITF) transport.

Table 2
Zonal Volume Transport Through the Major Oceanic Gateways

Zonal volume transport (Sv)	Panama seaway	Tethys seaway	Indonesian gateway	Drake passage	Tasman gateway	South African gateway
CCSM3_F	7.0	-11.3	-13.5	136.3	156.8	154.6
CCSM3_H	0.6	-11.3	-25.3	91.6	117.5	103.5
CCSM4	-1.2	-5.7	-18.7	209.9	227.4	214.4
CESM1	-3.2	-6.1	-18.8	212.1	227.6	214.9
IPSLCM5	7.5	0.0	-12.7	82.1	102.1	89.3
IPSLCM5_T	3.7	-3.7	-15.1	82.9	101.6	90.1
HadCM3L_B1	11.2	0.0	-10.8	116.5	138.5	127.7
HadCM3L_B2	11.5	0.0	-10.9	130.1	152.5	141.6
HadCM3L_F1	12.6	0.0	4.3	87.6	95.9	100.2
HadCM3L_F2	12.4	0.0	3.8	96.1	104.7	108.5
HadCM3L_F3	14.5	0.0	-8.2	90.1	112.8	104.6
HadCM3L_L1	7.2	0.0	-7.3	104.8	119.3	112.0
COSMOS	-8.0	-7.5	-20.9	140.9	153.7	140.3
GISS-E2.1	2.1	-2.5	-14.1	172.4	186.0	175.0

Note. The green shading highlights positive (eastward) transport and the red shading highlights negative (westward) values. The units are in Sverdrups ($10^6 \text{ m}^3/\text{s}$).

4.1. Tropical Gateways

The Panama Seaway was a tropical connection between the North Atlantic and the North Pacific that allowed the exchange of warm, salty waters (Huguet et al., 2022). Geochemical paleoceanographic tracers support a narrowing of the seaway throughout the Miocene, with it shoaling sufficiently to restrict Pacific inflow by ~ 9 Ma (Kirillova et al., 2019). Geological evidence indicates that the Isthmus of Panama formed by ~ 2.8 Ma, joining the Americas for terrestrial biological gene flow but ending surface water exchange between the tropical Atlantic and Pacific (O’Dea et al., 2016). However, it should be noted that some studies suggest partial or episodic restriction and shoaling of the Panama Seaway by the middle Miocene or earlier (Montes et al., 2015; Ramirez et al., 2016).

The Panama Seaway is open but differs substantially in depth and latitudinal extent in all the simulations (Figure 4a). The latitudinal position of the gateway in our simulations varies between 5°N and 13°N and the depth varies between ~ 500 and $\sim 4,000$ m (Table 1). The zonal volume transport through the Panama Seaway varies between -8 and 14.5 Sv (Figures 4b, Table 2), excluding HadCM3L_L1 because its latitudinal transect results in zero zonal VT. The positive values indicate eastward net transport, into the Atlantic, and the negative values indicate westward net transport, into the Pacific. Four of the five simulations with the deepest gateways have either no transport or a westward transport (into the Pacific) through the strait while the simulations with a shallower gateway ($\leq 1,200$ m) all have eastward transport (into the Atlantic) through the strait (Figure 4b). This may be related to the cross-section in other straits, which we investigate below. Broadly, as the Panama Seaway shoals, the transport turns from westward to eastward. In the simulations with the total VT across Panama Seaway close to zero, substantial exchange of water-mass still exists, however the total transport is close to zero due to opposing directions of flow at different depth levels which compensate the other (Figure S6 in Supporting Information S1).

The timing of the closure of the Tethys Seaway and its effects on global circulation have been widely debated with the timing of closure ranging from ~ 35 Ma to ~ 13 Ma (Allen & Armstrong, 2008; Bialik et al., 2019; Sun et al., 2021). The Tethys Seaway is only open in 7 of the 14 simulations and its cross-section area varies between them (Figure 5). The cross-section is computed across the narrowest and shallowest section of the Tethys Sea as this will control the volume transport across the seaway. This section is present in the Eastern Tethys Sea for 4 of the 7 simulations with CCSM3_F, GISS-E2.1, and COSMOS having a shallower Western Tethys. The depth of the cross-section is between ~ 120 and 800 m. The westward volume transport through the Tethys Seaway reduces with a reduction in area of the gateway across the simulations, except for GISS-E2.1 which has a weak VT (-2.5 Sv) even with a larger cross-section area of the Tethys Seaway (Figure 5b). The negative values of volume transport indicate it is always from the Indian Ocean into the Atlantic Ocean with values ranging between ~ -2.5 to -11 Sv.

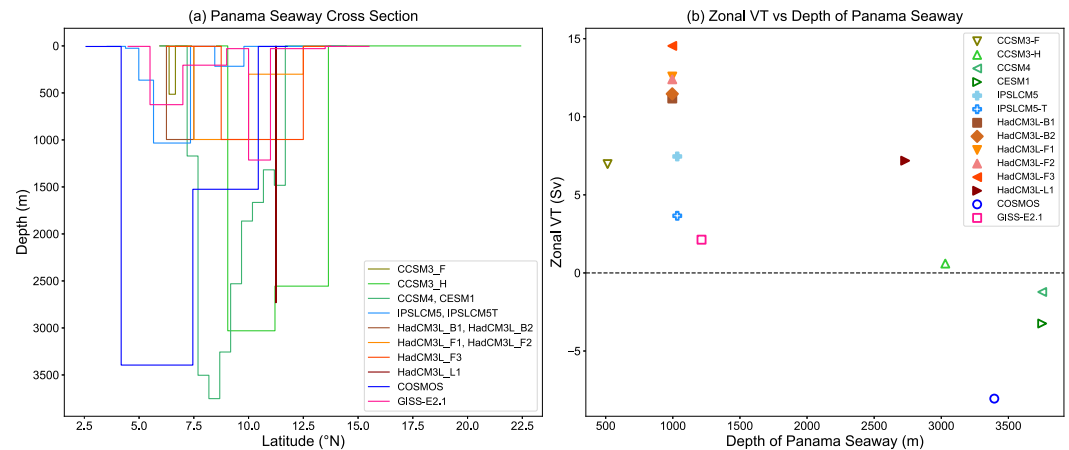


Figure 4. (a) The cross sections of the Panama Seaway in the simulations with depth on the Y-axis and the latitudinal position on the X-axis. (b) The relationship between the depth of the gateway (X-axis) and the volume transport across it (Y-axis). The unfilled symbols in panel (b) denote an open Tethys Seaway and the filled symbols denote a closed Tethys Seaway in that simulation. Here, we use the depth of the Panama Seaway as we want to investigate the effect of shoaling of the seaway on the zonal volume transport. The dashed line divides the transport into positive and negative values, which mean transport into the Atlantic and the Pacific respectively. Some simulations use the same paleogeographies so their gateway geometry is the same, for example, IPSL5CM5 and IPSL5CM5_T and they appear as a single cross section in 4a. The cross-section for HadCM3L_L1 is taken along the latitude instead of longitudinally, thus it appears as a straight line in 4a.

Several studies have reported that the closure of the Tethys Seaway and the cessation of the Tethyan Current may have led to the change in the direction of volume transport across the Panama Seaway from a net VT into the Pacific to the Atlantic (Omta & Dijkstra, 2003; von der Heydt & Dijkstra, 2005; von der Heydt & Dijkstra, 2006). In simulations with a closed Tethys Seaway, the transport across Panama Seaway is always positive (eastward into the Atlantic) (Figure 6). Furthermore, for all simulations where Panama Seaway transport is negative (westward into the Pacific), the Tethys is open. However, for simulations with an open Tethys Seaway (simulations with non-zero Tethys VT in Figure 6), the Panama VT is not always negative. Broadly, Panama VT turns increasingly positive as the Tethys VT reduces except in the case of CCSM3_H and CCSM3_F, which have the strongest Tethys VT but almost zero and significant positive Panama VT, respectively.

The island rule formulation introduced by Godfrey (1989) has been used to explain the reversal of Panama Seaway transport, where the reduction of Tethys Seaway VT and a simultaneous increase in Drake Passage VT led to the

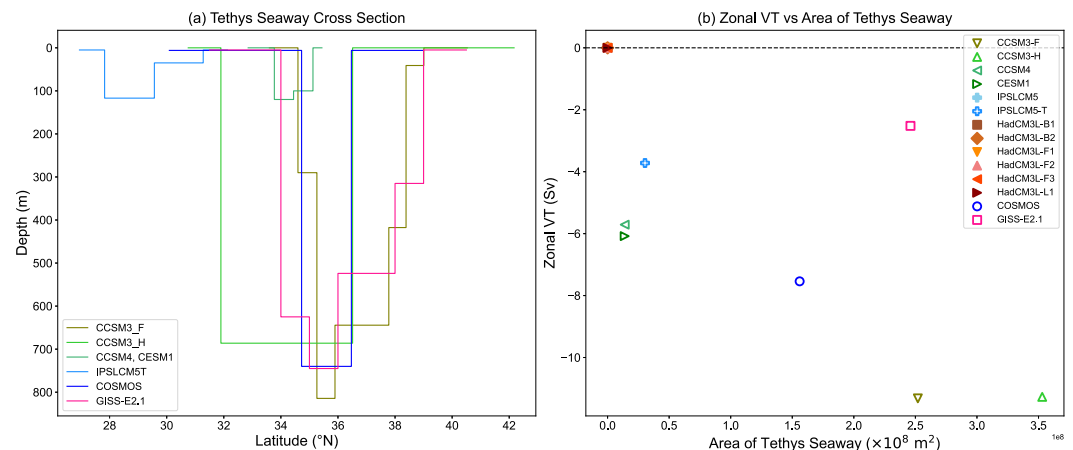


Figure 5. (a) The cross sections of the narrowest section of the Tethys Seaway in the models with depth on the Y-axis and the latitudinal position on the X-axis. (b) The relationship between the area of the gateway (X-axis) and the volume transport across it (Y-axis). The negative values indicate transport toward the west. Only 7 of the 14 models have an open Tethys Seaway.

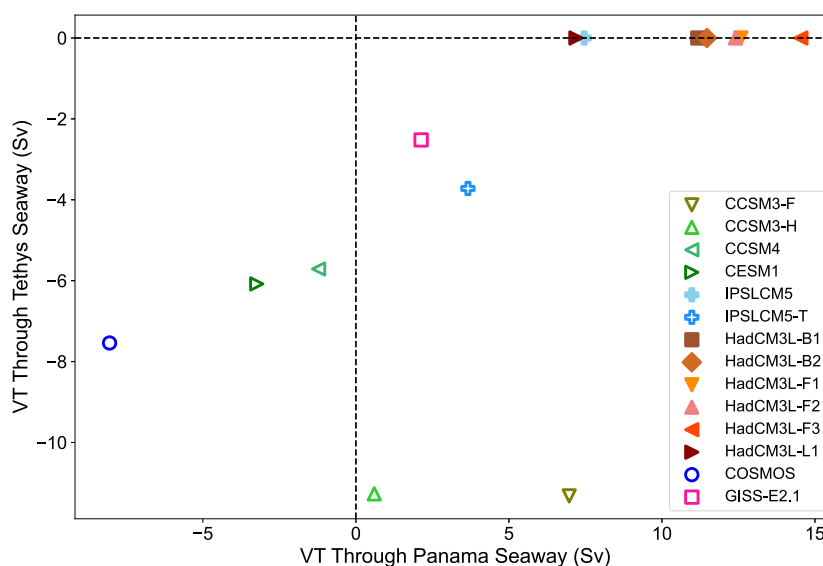


Figure 6. The zonal volume transport (VT) across Tethys Seaway versus the zonal VT across Panama Seaway. The negative sign for Tethys transport (Y-axis) indicates transport into the Atlantic and the same for Panama Seaway indicates transport into the Pacific. Positive values of Panama Seaway VT indicate transport into the Atlantic. Simulations with a closed Tethys Seaway have 0 Sv Tethys VT.

reversal of Panama VT from net Pacific to net Atlantic (Omta & Dijkstra, 2003; von der Heydt & Dijkstra, 2005). Here, South America was the island (due to an open Panama Seaway) around which the integral was calculated. The island rule formula is explained in Text S1 in Supporting Information S1, along with a comparison of the simulated Panama Seaway VT and that predicted by theory (Figure S7 in Supporting Information S1), and the values of all the terms involved in the formula presented in Table S1 in Supporting Information S1. There is no correlation between the predicted VT and the simulated VT. Except for two simulations, the Miocene simulations exhibit a Panama VT that gradually turns from negative to positive as the Tethys VT reduces (Figure 6). This follows well with the flow reversal mechanism described previously (Omta & Dijkstra, 2003; von der Heydt & Dijkstra, 2006). However, direct calculations of individual terms using this rule do not result in accurate estimates of Panama VT except for a few simulations (Figure S7 and Table S1 in Supporting Information S1). This could be because the previous studies used a barotropic model (Omta & Dijkstra, 2003) or a flat bathymetry (von der Heydt & Dijkstra, 2006), unlike the simulations used in this study. The island rule model assumes a level of no motion below which the ocean is considered to be stagnant; it assumes an unrestricted pathway around the island above this level of no motion, which is not the case when there are shallow straits around the island, which might add bottom drag.

Miocene ITF transport in most of the simulations is negative (Table 2), similar to its modern-day transport. However, in HadCM3L_F1 and HadCM3L_F2, the ITF VT is positive, unlike the other simulations in the HadCM3 family. The cross-section of the Indonesian Gateway's zonal velocity (Figure S8 in Supporting Information S1) reveals that HadCM3L_F1 and HadCM3L_F2 have a deeper and wider gateway, with most of the lower transport being positive, without any negative transport in the upper layers to counteract it, which is the case in the other HadCM3 simulations. Hence, the total VT in these two simulations is positive. Deeper levels of the gateway predominantly show positive zonal velocities across the simulations (Figure S7 in Supporting Information S1); however, the total VT does not exhibit a correlation with the depth of the gateway (not shown). Thus, the wind-driven section of the flow is controlling the total VT across the Indonesian Gateway.

4.2. Drake Passage

The Drake Passage is open in all the simulations (Figure 7), but there is a vast range in the volume transport across it, from 82 to 212 Sv (Table 2). CCSM4 and CESM1 have exceptionally high VT across the Drake Passage of about 209 and 212 Sv respectively, which is considerably higher than the modern observed value (155 ± 3 Sv; Artana et al., 2021). The depth of the Drake Passage in the simulations also has a wide range, from $\sim 2,000$ m to $\sim 4,000$ m (Figure 7a), which is shallower than its modern depth of $\sim 4,000$ – $5,000$ m (Bohoyo et al., 2019).

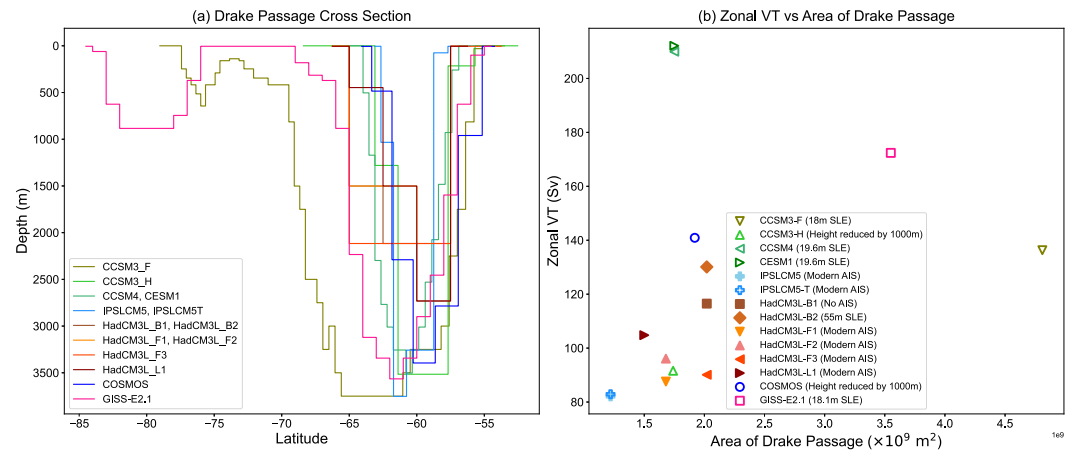


Figure 7. (a) The cross sections of the Drake Passage in the models with depth on the Y-axis and the latitudinal position on the X-axis. (b) The relationship between the area of the gateway (X-axis) and the volume transport across it (Y-axis).

CCSM3_F and GISS-E2.1 have a much wider Drake Passage than the other simulations, but the volume transport does not respond linearly to the area of the passage between the simulations (Figure 7b). The zonal VT across the Drake Passage increases as a result of the addition of the AIS, which can be seen in the case of HadCM3L_B1 and HadCM3L_B2 where the former has no AIS while the latter simulation includes a modern-like AIS (Figure 7b). A similar mechanism of an increase in Drake passage transport due to addition of an AIS was reported in Ladant et al. (2014), where they found that adding an AIS led to an increase in sea ice and subsequently stronger meridional density gradients and increased VT. An increase in the CO₂ level also leads to an increase in the transport, seen in the case of HadCM3L_F1 (400 ppm) and HadCM3L_F2 (760 ppm). The Tethys Seaway being open or closed makes no difference as the IPSLCM5 (Tethys Seaway closed) and IPSLCM5_T (Tethys Seaway—120 m) simulations show almost the same zonal VT. It has been suggested that a brief constriction of the Drake Passage around ~26 to 14 Ma could have resulted in the weakening of the ACC (Lagabrielle et al., 2009), which has been linked to a subsequent weakening in the MOC (Toyos et al., 2020). Our results do not indicate this, and it could mean that the strength of the ACC is more dependent on other aspects of the simulations, like the Antarctic ice sheet and its influence on the meridional temperature gradient across the passage, which we investigate next.

4.3. ACC Transport

The timing of the onset of the ACC and its strengthening to modern levels is a highly debated topic among the paleoclimate community, with the opening of the Tasmanian Gateway and Drake Passage being the main constraints (Barker et al., 2007). Both were likely open and deep by the Miocene, although some studies suggest a restriction of the Drake Passage around the early to middle Miocene (Lagabrielle et al., 2009; Martos et al., 2013). With unrestricted latitudinal bands in the ACC region, the major control over the variability in ACC transport is provided by changes in the westerly zonal maximum wind stress and meridional density gradients (Munday et al., 2015; Olbers et al., 2004). We investigate the dependence of the ACC on the maximum zonal westerly wind stress over the Southern Ocean and the meridional density difference across the different simulations (Figure 8). The ACC transport here is defined as the difference in the barotropic streamfunction values across the Drake Passage. The Southern Hemisphere wind stress (SH τ_x) is defined as the maximum of zonal average wind stress over the Southern Ocean and the meridional density difference ($\Delta\rho_y$) is calculated as the difference in the mean potential density (referenced to 2,000 dbar) between 42–45°S and 62–65°S averaged over 0–1,500 m following Kuhlbrodt et al. (2012). The ACC transport is equated to the transport through the Drake Passage here, since it is the minimum transport of the three gateways around Antarctica (Table 2) and as such represents the core of the ACC. For the Miocene simulations, ACC transport shows weak positive correlation with SH τ_x ($r = 0.4$, $p = 0.15$), which is not statistically significant at the 95% confidence level (Figure 8a). The relationship with $\Delta\rho_y$ is moderately negative ($r = -0.52$, $p = 0.059$), which approaches statistical significance, suggesting that density gradients may have exerted some control on ACC transport (Figure 8d). When the three strongest-transport models (viz., CCSM4, CESM1 and GISS-E2.1) are excluded, the correlation with SH τ_x strengthens considerably ($r = 0.74$, $p = 0.0095$), indicating a statistically significant and robust dependence on wind stress once

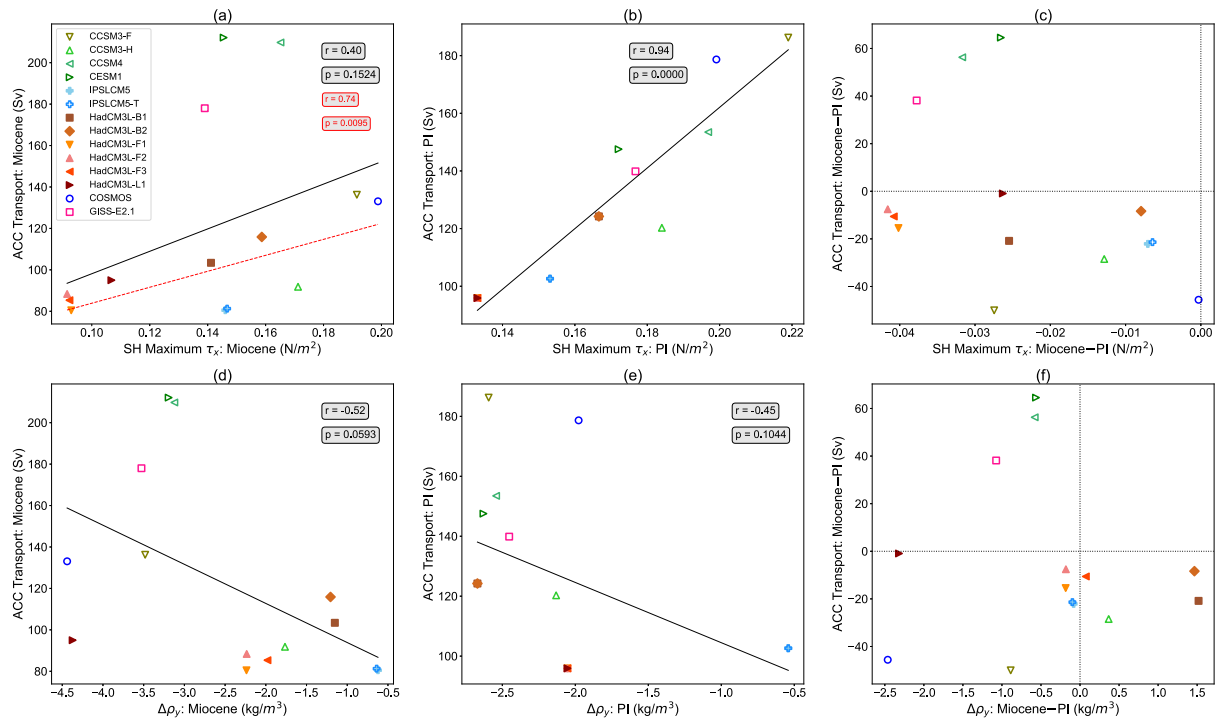


Figure 8. (a) ACC transport during the Miocene versus the maximum zonal wind stress over the Southern Ocean (SH, τ_x) (N m^{-2}). (b) PI ACC transport (Sv) versus SH τ_x (N m^{-2}). (c) The difference in the ACC transport between Miocene and PI versus the difference in maximum westerly wind stress. (d) Miocene: ACC transport versus meridional density difference ($\Delta\rho_y$) (kg m^{-3}). The meridional density difference is calculated as the difference in average potential density (referenced to 2,000 dbar) between 42–45°S and 62–65°S, averaged over 0–1,500 m. (e) PI: ACC transport versus $\Delta\rho_y$. (f) The difference in the ACC transport between Miocene and PI versus the difference in $\Delta\rho_y$. The gray boxes in (a, b, d, and e), are the Pearson correlation coefficient “ r ” and the p -value “ p ”. The red boxes in (a) show “ r ” and “ p ” for all the simulations excluding CCSM4, CESM1 and GISS-E2.1, which have Miocene ACC transport of more than 150 Sv.

these outliers are removed (as shown in Figure 8a by the red boxes and the dashed red line showing the regression excluding these three simulations). Compared to PI, the ACC transport is weaker in most of the Miocene simulations (Figure 8c), except in CCSM4, CESM1, and GISS-E2.1. These three simulations have a weaker τ_x during the Miocene compared to PI (Figure 8c), but a stronger $\Delta\rho_y$ (Figure 8f; here, negative value of Miocene-PI $\Delta\rho_y$ means Miocene $\Delta\rho_y$ is stronger since $\Delta\rho_y$ is negative). This stronger density gradient in the Miocene possibly led to a stronger simulated ACC. This stronger $\Delta\rho_y$ could result from a stronger temperature gradient (Figure S9c in Supporting Information S1), although other simulation show stronger gradients. This suggests that in CCSM4, CESM1, and GISS-E2.1, the Miocene ACC response is more sensitive to density gradients than to wind stress, possibly due to model physics.

5. Summary and Discussion

In this study, we explore the gyre circulation and gateway volume transport during the early and middle Miocene using 14 fully coupled climate model simulations. Our findings reveal interesting impacts of different paleogeography on the oceanic gyres and wind stress. The barotropic streamfunctions (Section 3) reveal that during the early and middle Miocene, the North Atlantic STG, especially in the Gulf Stream region, and SPG were weaker than PI. On the other hand, the North Pacific STG and SPG were stronger than PI. The strengthening or weakening of gyre transport largely follows the strengthening or weakening of wind stress curl, respectively, acting over the basins (Figures 3a, 3d, 3f, and 3i), as also observed for the Eocene by Zhang et al. (2025). Along with the wind stress curl, the narrower Atlantic and the wider Pacific in the Miocene simulations, likely contributed to the gyre strength changes (Figures 3b, 3e, 3g, and 3j; Jones & Cessi, 2017; Pierini, 2008; Sverdrup, 1947). The detailed reasons for changes in wind stress are outside the scope of this study, though, two mechanisms are likely. Firstly, the Australian continent was situated further south in the Miocene compared to modern-day and may have contributed to altering the wind stress distribution through topographic form stress

changes as was the case for the Eocene (Zhang et al., 2020, 2025). Secondly, Miocene sea level pressure indicates a lowering of the pressure in the North Pacific low-pressure zone compared to PI (Figure S10c in Supporting Information S1). This resulted in an increase in the meridional pressure gradient across the North Pacific, which is likely the reason for stronger Miocene mid-latitude surface westerlies over the North Pacific (Figure 3h).

Overall, our Miocene simulations lie somewhere between the Eocene and the present day in terms of gyre strengths and the wind stress pattern, since in the Eocene, the Atlantic gyres are much weaker, and South Pacific STG is much stronger compared to PI and Miocene simulations, due to the large differences in continental positions and gateways (Zhang et al., 2020). The Eocene North Pacific gyres were only slightly stronger than or comparable to PI (Zhang et al., 2025). By the Miocene, the continents were closer to their modern positions, hence the gyre circulation had likely started to develop toward its modern structure by this time, as described above, except in the tropics with open gateways.

The open low-latitude gateways in the Miocene may have facilitated a low-latitude circumglobal current and thus altered the gyre circulation as well. We examined the theories that try to explain the interdependence of transport through the Tethys and Panama Seaways using the island rule (Godfrey, 1989). These theories postulate that as the Tethys VT weakens and the Drake VT increases, the VT through Panama Seaway changes from net Pacific VT (westwards) to net Atlantic VT (eastwards) (Omta & Dijkstra, 2003; von der Heydt & Dijkstra, 2005). We find that most of our simulations approximately follow this theory, with the Panama VT turning increasingly eastward with a declining westwards Tethys VT (Figure 6). In simulations with a closed Tethys Seaway, the Panama VT is always eastwards, but for simulations with an open Tethys Seaway, it may depend on the depth of the Panama Seaway. The transport through the Drake Passage also plays a role in the direction of flow through the Panama Seaway. Strong Drake VT may lead to a positive Panama VT even with a strong westward Tethys VT. With a Panama Seaway which may be shallower than the level of no motion, the island rule calculation of the expected westward flow through Panama Seaway is not observed. Nof and Van Gorder (2003) suggested that a positive VT across Panama Seaway is only possible if there is weak deep water formation in the North Atlantic. However, comparing the AMOC values from Naik, Boer, Coxall, et al. (2025) to the Panama VT, we find a strong positive VT even in the two simulations with the strongest AMOC.

An amendment added to the island rule, which includes the effects of overturning circulation through upwelling in the interior Pacific Ocean, allows for a better estimation of ITF transport in the modern ocean (Feng et al., 2017). Thus, the island rule in its original formulation, without the effects of deep circulation included, may not be accurate for estimating transport around islands. The progression of the transport in Panama and Tethys went from all westwards in the early Miocene, followed by the closure of the Tethys Seaway, when the Tethys transport ceased, and Panama VT turned eastward. While with an open Tethys, an eastward Panama VT was possible if the Panama Seaway was shallow, most recent studies suggest that the Tethys Seaway closed before (~13 Ma) the critical shoaling of the Panama Seaway (~9 Ma) (Bialik et al., 2019; Kirillova et al., 2019; Sun et al., 2021). Thus, the former is the most likely scenario for the progression of the tropical transports, as our simulations suggest.

Miocene ACC transport generally increases with increasing wind stress across the simulations, except for the three simulations with the strongest ACC transport which have moderately strong westerly wind stress maxima (Figure 8a). In those three cases, the simulated ACC in the Miocene is stronger than PI. This might be caused by an increased density gradient across the ACC in the Miocene compared to PI (Figure 8f), likely a result of an increased temperature gradient (Figure S9c in Supporting Information S1). However, we note that these gradients are only moderately stronger than in other models, and the differing behavior of CCSM4, CESM1, and GISS-E2.1 likely also reflects model-dependent sensitivities. Previous studies have shown that ACC transport is strongly affected by viscosity (Jochum et al., 2008), eddy parameterization schemes (Kuhlbrodt et al., 2012), and other aspects of model physics. In paleoclimate simulations, boundary condition changes and parameter adjustments may further alter ACC sensitivity. Thus, the stronger ACC in these three models probably results from a combination of buoyancy forcing and model-physics factors.

Recent work focused on the past 5 Myr has shown that stronger-than-modern ACC transport can occur even in the absence of peak westerly wind stress, suggesting that enhanced oceanic density gradients may play a central role (Lamy et al., 2024). Interestingly, this is consistent with our Miocene results, where the strongest ACC transport occurs in cases with only moderately strong wind stress but likely increased meridional density gradients. This points toward the possibility that similar mechanisms may have been active in both the Pliocene and Miocene. This highlights the need to extend reconstructions of ACC dynamics further back into the Miocene, which would

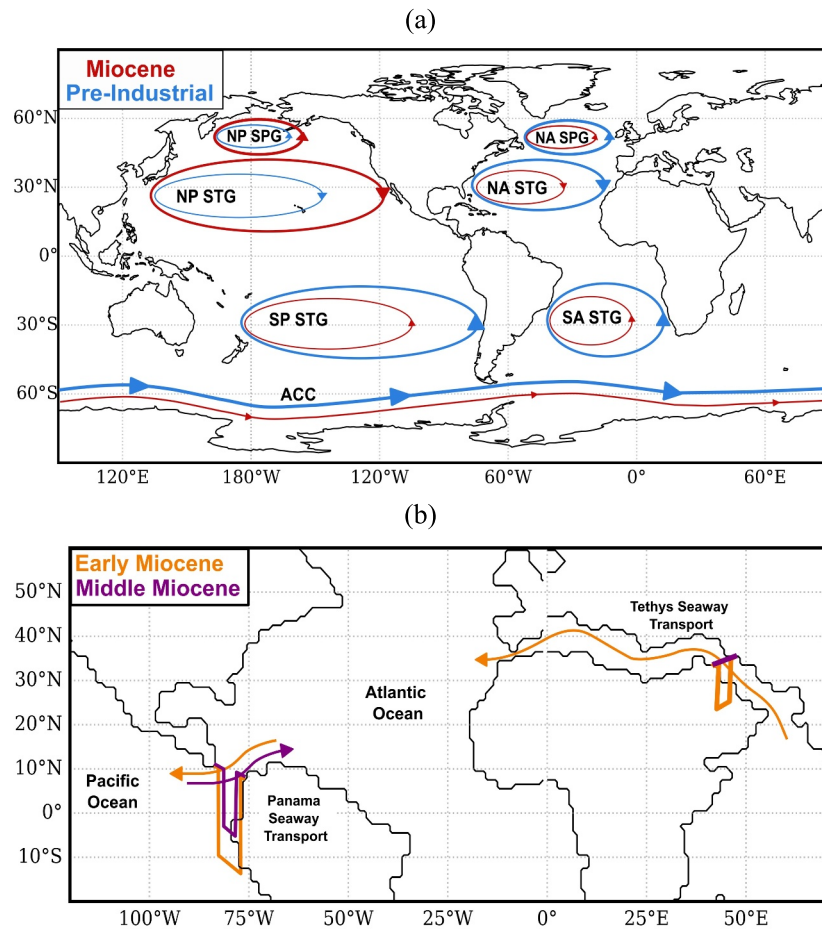


Figure 9. Summary of the main results of the study. (a) In the Miocene (red) simulations, gyres were weaker in the Atlantic and South Pacific, while the North Pacific gyres were stronger compared to pre-industrial (PI) (blue). Antarctic Circumpolar Current (ACC) transport was weaker in the Miocene (red) compared to PI (blue). NA—North Atlantic, NP—North Pacific, SA—South Atlantic, SP—South Pacific, SPG—Subpolar Gyre, STG—Subtropical Gyre. (b) Panama Seaway transport was westward (Atlantic to Pacific) in the early Miocene (orange) when the Panama Seaway was deep and the Tethys Seaway was open. During the middle Miocene (purple), when the Tethys Seaway closed and the Panama Seaway shoaled, volume transport through the Panama Seaway turned eastward (Pacific to Atlantic).

be valuable for better constraining the long-term evolution of Southern Ocean circulation and its drivers. Nonetheless, our simulations indicate that Southern Hemisphere westerlies, and therefore the ACC, were weaker than modern during the Miocene, consistent with proxy evidence for a reduced latitudinal temperature gradient across the Southern Ocean that likely contributed to weaker winds (Holbourn et al., 2024). Simulated Miocene sea level pressure is higher in the Southern Ocean low-pressure belt compared to PI (Figure S10 in Supporting Information S1). This led to a weaker pressure gradient and thus, likely contributed to the weaker westerlies.

In conclusion, we analyzed 14 fully coupled climate model simulations of the early and middle Miocene to investigate gyre circulation and gateway volume transport. The main conclusions are highlighted in Figure 9. We find that the North Atlantic gyres were weaker than in PI, while the North Pacific gyres were stronger. ACC transport was slightly weaker overall, though a few simulations show stronger-than-PI values, likely driven by enhanced meridional density gradients rather than peak wind stress. These differences are primarily linked to changes in wind stress patterns, shaped by a lower meridional temperature gradient and distinct Miocene paleogeography. We also explored the interdependence of low-latitude gateway transports using the island rule. In general, our results support a progression from westward to eastward Panama Seaway flow as the Tethys Seaway closed, although this might be masked in some simulations due to different widths of the Drake Passage

and different wind stress patterns. While the Miocene ITF cross-section was deep, the negative VT (Pacific to Indian Ocean) across it was predominantly set by the upper wind-driven section of the gateway transport.

Overall, our findings emphasize that Miocene circulation patterns reflect a circulation between the Eocene and modern configurations. They also underscore the value of extending ACC and gateway reconstructions into the Miocene to better understand long-term ocean circulation changes and their climate impacts.

Conflict of Interest

The authors declare no conflicts of interest relevant to this study.

Data Availability Statement

The data set used to create the figures in this manuscript is available at Naik, Boer, Burls, et al. (2025). The Python code to make the figures is available at (Naik, 2025).

Acknowledgments

TJN acknowledges funding from Stockholm University Department of Geological Sciences and the Bolin Centre for Climate Research. AdB was supported by VR Grant 2020-04791. NJB acknowledges funding support from NSF awards AGS-1844380 and EAR-2303417. MH acknowledges support from NSF OCE 2217530, “Collaborative Research: NSFGE0-NERC: Solving the conundrum of the Miocene South Asian Monsoon.” ANL thanks the NASA Center for Climate Simulation and NASA GISS for institutional support. DJL acknowledges NERC grant NE/X000222/1. YZ was supported by the National Key Research and Development Program of China (2023YFF0803902).

References

- Allen, M. B., & Armstrong, H. A. (2008). Arabia–Eurasia collision and the forcing of mid-Cenozoic global cooling. *Paleogeography, Paleoclimatology, Paleoecology*, 265(1–2), 52–58. <https://doi.org/10.1016/j.palaeo.2008.04.021>
- Aoki, K., & Kutsuwada, K. (2008). Verification of the wind-driven transport in the North Pacific subtropical gyre using gridded wind-stress products. *Journal of Oceanography*, 64(1), 49–60. <https://doi.org/10.1007/s10872-008-0004-6>
- Artana, C., Ferrari, R., Bricaud, C., Lellouche, J.-M., Garric, G., Sennéchaël, N., et al. (2021). Twenty-five years of Mercator ocean reanalysis GLORYS12 at drake passage: Velocity assessment and total volume transport. *Advances in Space Research*, 68(2), 447–466. (25 Years of Progress in Radar Altimetry). <https://doi.org/10.1016/j.asr.2019.11.033>
- Barker, P. F., Filippelli, G. M., Florindo, F., Martin, E. E., & Scher, H. D. (2007). Onset and role of the Antarctic circumpolar current. *Deep Sea Research Part II: Topical Studies in Oceanography*, 54(21–22), 2388–2398. <https://doi.org/10.1016/j.dsr2.2007.07.028>
- Bialik, O. M., Frank, M., Betzler, C., Zammit, R., & Waldmann, N. D. (2019). Two-step closure of the Miocene Indian Ocean gateway to the Mediterranean. *Scientific Reports*, 9(1), 8842. <https://doi.org/10.1038/s41598-019-45308-7>
- Bohoyo, F., Larter, R. D., Galindo-Zaldívar, J., Leat, P. T., Maldonado, A., Tate, A. J., et al. (2019). Morphological and geological features of drake passage, Antarctica, from a new digital bathymetric model. *Journal of Maps*, 15(2), 49–59. <https://doi.org/10.1080/17445647.2018.1543618>
- Böning, C. W., Scheinert, M., Dengg, J., Biastoch, A., & Funk, A. (2006). Decadal variability of subpolar gyre transport and its reverberation in the North Atlantic overturning. *Geophysical Research Letters*, 33(21). <https://doi.org/10.1029/2006GL026906>
- Bradshaw, C. D., Langebroek, P. M., Lear, C. H., Lunt, D. J., Coxall, H. K., Sosdian, S. M., & de Boer, A. M. (2021). Hydrological impact of middle Miocene Antarctic ice-free areas coupled to deep ocean temperatures. *Nature Geoscience*, 14(6), 429–436. <https://doi.org/10.1038/s41561-021-00745-w>
- Brierley, C. M., & Fedorov, A. V. (2016). Comparing the impacts of Miocene–Pliocene changes in inter-ocean gateways on climate: Central American seaway, Bering Strait, and Indonesia. *Earth and Planetary Science Letters*, 444, 116–130. <https://doi.org/10.1016/j.epsl.2016.03.010>
- Burls, N. J., Bradshaw, C. D., De Boer, A. M., Herold, N., Huber, M., Pound, M., et al. (2021). Simulating Miocene warmth: Insights from an opportunistic multi-model ensemble (MioMIP1). *Paleoceanography and Paleoclimatology*, 36(5), e2020PA004054. <https://doi.org/10.1029/2020PA004054>
- De Boer, A. M., Graham, R. M., Thomas, M. D., & Kohfeld, K. E. (2013). The control of the Southern Hemisphere westerlies on the position of the subtropical front. *Journal of Geophysical Research: Oceans*, 118(10), 5669–5675. <https://doi.org/10.1002/jgrc.20407>
- Drouin, K. L., Lozier, M. S., & Johns, W. E. (2021). Variability and trends of the south Atlantic subtropical gyre. *Journal of Geophysical Research: Oceans*, 126(1), e2020JC016405. <https://doi.org/10.1029/2020JC016405>
- Ehlers, B.-M., & Jokat, W. (2013). Paleo-bathymetry of the northern North Atlantic and consequences for the opening of the Fram Strait. *Marine Geophysical Researches*, 34(1), 25–43. <https://doi.org/10.1007/s11001-013-9165-9>
- Farnsworth, A., Lunt, D. J., O'Brien, C. L., Foster, G. L., Inglis, G. N., Markwick, P., et al. (2019). Climate sensitivity on geological timescales controlled by nonlinear feedbacks and ocean circulation. *Geophysical Research Letters*, 46(16), 9880–9889. <https://doi.org/10.1029/2019GL083574>
- Feng, M., Zhang, X., Sloyan, B., & Chamberlain, M. (2017). Contribution of the deep ocean to the centennial changes of the Indonesian throughflow. *Geophysical Research Letters*, 44(6), 2859–2867. <https://doi.org/10.1002/2017GL072577>
- Ferrari, R., & Ferreira, D. (2011). What processes drive the ocean heat transport? *Ocean Modelling*, 38(3), 171–186. <https://doi.org/10.1016/j.ocmod.2011.02.013>
- Frigola, A., Prange, M., & Schulz, M. (2018). Boundary conditions for the middle miocene climate transition (MMCT v1.0). *Geoscientific Model Development*, 11(4), 1607–1626. <https://doi.org/10.5194/gmd-11-1607-2018>
- Gallagher, S. J., Auer, G., Brierley, C. M., Fulthorpe, C. S., & Hall, R. (2024). Cenozoic history of the Indonesian gateway. *Annual Review of Earth and Planetary Sciences*, 52(1), 581–604. <https://doi.org/10.1146/annurev-earth-040722-111322>
- Gladenkov, A. Y. (2004). Onset of connections between the Pacific and Arctic Oceans through the Bering Strait in the Neogene.
- Godfrey, J. (1989). A sverdrup model of the depth-integrated flow for the world ocean allowing for island circulations. *Geophysical & Astrophysical Fluid Dynamics*, 45(1–2), 89–112. <https://doi.org/10.1080/03091928908208894>
- Gray, W. R., Wills, R. C. J., Rae, J. W. B., Burke, A., Ivanovic, R. F., Roberts, W. H. G., et al. (2020). Wind-driven evolution of the North Pacific subpolar gyre over the last deglaciation. *Geophysical Research Letters*, 47(6), e2019GL086328. <https://doi.org/10.1029/2019GL086328>
- Hall, J. R., Allison, M. S., Papadopoulos, M. T., Barfod, D. N., & Jones, S. M. (2023). Timing and consequences of Bering Strait opening: New insights from ⁴⁰Ar/³⁹Ar dating of the Barmur group (Tjörnes beds), northern Iceland. *Paleoceanography and Paleoclimatology*, 38(4), e2022PA004539. <https://doi.org/10.1029/2022PA004539>

- Herold, N., Huber, M., & Müller, R. D. (2011). Modeling the Miocene climatic optimum. Part I: Land and atmosphere. *Journal of Climate*, 24(24), 6353–6372. <https://doi.org/10.1175/2011JCLI4035.1>
- Herold, N., Seton, M., Müller, R., You, Y., & Huber, M. (2008). Middle Miocene tectonic boundary conditions for use in climate models. *Geochemistry, Geophysics, Geosystems*, 9(10). <https://doi.org/10.1029/2008GC002046>
- Hodel, F., Grespan, R., de Rafélis, M., Dera, G., Lezin, C., Nardin, E., et al. (2021). Drake Passage gateway opening and Antarctic circumpolar current onset 31 Ma ago: The message of Foraminifera and reconsideration of the neodymium isotope record. *Chemical Geology*, 570, 120171. <https://doi.org/10.1016/j.chemgeo.2021.120171>
- Holbourn, A., Kuhnt, W., Kulhanek, D. K., Mountain, G., Rosenthal, Y., Sagawa, T., et al. (2024). Re-organization of Pacific overturning circulation across the Miocene climate optimum. *Nature Communications*, 15(1), 8135. <https://doi.org/10.1038/s41467-024-52516-x>
- Hossain, A., Knorr, G., Jokat, W., & Lohmann, G. (2021). Opening of the fram strait led to the establishment of a modern-like three-layer stratification in the Arctic Ocean during the Miocene. *arktos*, 7(1–3), 1–12. <https://doi.org/10.1007/s41063-020-00079-8>
- Hossain, A., Knorr, G., Lohmann, G., Stärr, M., & Jokat, W. (2020). Simulated thermohaline fingerprints in response to different Greenland-Scotland Ridge and fram strait subsidence histories. *Paleoceanography and Paleoclimatology*, 35(7), e2019PA003842. <https://doi.org/10.1029/2019PA003842>
- Huber, M., Brinkhuis, H., Stickley, C. E., Döös, K., Sluijs, A., Warnaar, J., et al. (2004). Eocene circulation of the Southern Ocean: Was Antarctica kept warm by subtropical waters? *Paleoceanography*, 19(4). <https://doi.org/10.1029/2004PA001014>
- Huguet, C., Jaeschke, A., & Rethemeyer, J. (2022). Paleoclimatic and palaeoceanographic changes coupled to the Panama Isthmus closing (13–4 Ma) using organic proxies. *Palaeogeography, Palaeoclimatology, Palaeoecology*, 601, 111139. <https://doi.org/10.1016/j.palaeo.2022.111139>
- Jakobsson, M., Backman, J., Rudels, B., Nycander, J., Frank, M., Mayer, L., et al. (2007). The early Miocene onset of a ventilated circulation regime in the Arctic Ocean. *Nature*, 447(7147), 986–990. <https://doi.org/10.1038/nature05924>
- Jochum, M., Danabasoglu, G., Holland, M., Kwon, Y. O., & Large, W. (2008). Ocean viscosity and climate. *Journal of Geophysical Research*, 113(C6). <https://doi.org/10.1029/2007jc004515>
- Jones, C. S., & Cessi, P. (2017). Size matters: Another reason why the Atlantic is saltier than the Pacific. *Journal of Physical Oceanography*, 47(11), 2843–2859. <https://doi.org/10.1175/JPO-D-17-0075.1>
- Judd, E. J., Tierney, J. E., Lunt, D. J., Montañez, I. P., Huber, B. T., Wing, S. L., & Valdes, P. J. (2024). A 485-million-year history of Earth's surface temperature. *Science*, 385(6715), eadk3705. <https://doi.org/10.1126/science.adk3705>
- Karami, M. (2011). *Paleoceanography of the Miocene Mediterranean Sea and Paratethys: Regional ocean modelling of the response to closure of the Tethys Seaway*. Utrecht University.
- Kirilova, V., Osborne, A. H., Störling, T., & Frank, M. (2019). Miocene restriction of the Pacific-North Atlantic throughflow strengthened Atlantic overturning circulation. *Nature Communications*, 10(1), 4025. <https://doi.org/10.1038/s41467-019-12034-7>
- Krapp, M., & Jungclaus, J. H. (2011). The middle Miocene climate as modelled in an atmosphere-ocean-biosphere model. *Climate of the Past*, 7(4), 1169–1188. <https://doi.org/10.5194/cp-7-1169-2011>
- Kuhlbrodt, T., Smith, R. S., Wang, Z., & Gregory, J. M. (2012). The influence of eddy parameterizations on the transport of the Antarctic circumpolar current in coupled climate models. *Ocean Modelling*, 52–53, 1–8. <https://doi.org/10.1016/j.ocemod.2012.04.006>
- Kuhnt, W., Holbourn, A., Hall, R., Zuvella, M., & Käse, R. (2004). Neogene history of the Indonesian throughflow. *Continents-Ocean Interactions within East Asian Marginal Seas. Geophysical Monograph*, 149, 299–320. <https://doi.org/10.1029/149gm16>
- Ladant, J. B., Donnadieu, Y., & Dumas, C. (2014). Links between CO₂, glaciation and water flow: Reconciling the Cenozoic history of the Antarctic circumpolar current. *Climate of the Past*, 10(6), 1957–1966. <https://doi.org/10.5194/cp-10-1957-2014>
- Lagabrielle, Y., Goddérís, Y., Donnadieu, Y., Malavieille, J., & Suarez, M. (2009). The tectonic history of Drake Passage and its possible impacts on global climate. *Earth and Planetary Science Letters*, 279(3–4), 197–211. <https://doi.org/10.1016/j.epsl.2008.12.037>
- Lamy, F., Winckler, G., Arz, H. W., Farmer, J. R., Gottschalk, J., Lembke-Jene, L., et al. (2024). Five million years of Antarctic circumpolar current strength variability. *Nature*, 627(8005), 789–796. <https://doi.org/10.1038/s41586-024-07143-3>
- Lunt, D. J., Dunkley Jones, T., Heinemann, M., Huber, M., LeGrande, A., Winguth, A., et al. (2012). A model–data comparison for a multi-model ensemble of early Eocene atmosphere–ocean simulations: EoMIP. *Climate of the Past*, 8(5), 1717–1736. <https://doi.org/10.5194/cp-8-1717-2012>
- Lunt, D. J., Valdes, P. J., Haywood, A., & Rutt, I. C. (2008). Closure of the Panama seaway during the Pliocene: Implications for climate and Northern hemisphere glaciation. *Climate Dynamics*, 30(1), 1–18. <https://doi.org/10.1007/s00382-007-0265-6>
- Markwick, P. (2007). The palaeogeographic and palaeoclimatic significance of climate proxies for data-model comparisons.
- Martos, Y. M., Maldonado, A., Lobo, F. J., Hernández-Molina, F. J., & Pérez, L. F. (2013). Tectonics and palaeoceanographic evolution recorded by contourite features in southern Drake Passage (Antarctica). *Marine Geology*, 343, 76–91. <https://doi.org/10.1016/j.margeo.2013.06.015>
- Montes, C., Bayona, G., Cardona, A., Buchs, D. M., Silva, C., Morón, S., et al. (2012). Arc-continent collision and orocline formation: Closing of the Central American seaway. *Journal of Geophysical Research*, 117(B4). <https://doi.org/10.1029/2011jgb008959>
- Montes, C., Cardona, A., Jaramillo, C., Pardo, A., Silva, J., Valencia, V., et al. (2015). Middle Miocene closure of the Central American seaway. *Science*, 348(6231), 226–229. <https://doi.org/10.1126/science.aaa2815>
- Morlighem, M., Williams, C. N., Rignot, E., An, L., Arndt, J. E., Bamber, J. L., et al. (2017). BedMachine v3: Complete bed topography and ocean bathymetry mapping of Greenland from multibeam echo sounding combined with mass conservation. *Geophysical Research Letters*, 44(21), 11051–11061. <https://doi.org/10.1002/2017GL074954>
- Munday, D. R., Johnson, H. L., & Marshall, D. P. (2015). The role of ocean gateways in the dynamics and sensitivity to wind stress of the early Antarctic circumpolar current. *Paleoceanography*, 30(3), 284–302. <https://doi.org/10.1002/2014PA002675>
- Munk, W. H. (1950). On the wind-driven ocean circulation. *Journal of the Atmospheric Sciences*, 7(2), 80–93. [https://doi.org/10.1175/1520-0469\(1950\)007<0080:OTWDOC>2.0.CO;2](https://doi.org/10.1175/1520-0469(1950)007<0080:OTWDOC>2.0.CO;2)
- Naik, T. (2025). Code for climate model output of Miocene ocean gyre circulation and gateway transports – MioMIP1 ocean intercomparison (version 1.0.0) [Software]. *Bolin Centre Code Repository*. <https://doi.org/10.57669/naik-2025-miomip1-gcgt-1.0.0>
- Naik, T., de Boer, A., Burls, N., Bradshaw, C., Donnadieu, Y., Farnsworth, A., et al. (2025). Climate model output of ocean gyre circulation and gateway transports for the early and middle Miocene — MioMIP1 (version 1) [Dataset]. *Bolin Centre Database*. <https://doi.org/10.17043/naik-2025-miomip1-gcgt-1>
- Naik, T. J., de Boer, A. M., Coxall, H. K., Burls, N. J., Bradshaw, C. D., Donnadieu, Y., et al. (2025). Ocean meridional overturning circulation during the early and middle Miocene. *Paleoceanography and Paleoclimatology*, 40(4), e2024PA005055. <https://doi.org/10.1029/2024PA005055>
- Newkirk, D. R., & Martin, E. E. (2009). Circulation through the central American seaway during the Miocene carbonate crash. *Geology*, 37(1), 87–90. <https://doi.org/10.1130/g25193a.1>

- Nof, D., & Van Gorder, S. (2003). Did an open Panama isthmus correspond to an invasion of Pacific water into the Atlantic? *Journal of Physical Oceanography*, 33(7), 1324–1336. [https://doi.org/10.1175/1520-0485\(2003\)033<1324:DAOPIC>2.0.CO;2](https://doi.org/10.1175/1520-0485(2003)033<1324:DAOPIC>2.0.CO;2)
- O’Dea, A., Lessios, H. A., Coates, A. G., Eytan, R. I., Restrepo-Moreno, S. A., Cione, A. L., et al. (2016). Formation of the isthmus of Panama. *Science Advances*, 2(8), e1600883. <https://doi.org/10.1126/sciadv.1600883>
- Ögretmen, N., Schiebel, R., Jochum, K. P., Stoll, B., Weis, U., Repschläger, J., et al. (2020). Deep thermohaline circulation across the closure of the central American seaway. *Paleoceanography and Paleoclimatology*, 35(12), e2020PA004049. <https://doi.org/10.1029/2020PA004049>
- Olbers, D., Borowski, D., Völker, C., & Wölff, J.-O. (2004). The dynamical balance, transport and circulation of the Antarctic circumpolar current. *Antarctic Science*, 16(4), 439–470. <https://doi.org/10.1017/S0954102004002251>
- Omta, A. W., & Dijkstra, H. A. (2003). A physical mechanism for the Atlantic–Pacific flow reversal in the early Miocene. *Global and Planetary Change*, 36(4), 265–276. [https://doi.org/10.1016/S0921-8181\(02\)00221-7](https://doi.org/10.1016/S0921-8181(02)00221-7)
- Palter, J. B. (2015). The role of the gulf stream in European climate. *Annual Review of Marine Science*, 7(1), 113–137. <https://doi.org/10.1146/annurev-marine-010814-015656>
- Pierini, S. (2008). On the crucial role of basin geometry in double-gyre models of the Kuroshio extension. *Journal of Physical Oceanography*, 38(6), 1327–1333. <https://doi.org/10.1175/2007JPO3924.1>
- Pillot, Q., Donnadieu, Y., Sarr, A. C., Ladant, J. B., & Suchéras-Marx, B. (2022). Evolution of ocean circulation in the North Atlantic Ocean during the Miocene: Impact of the Greenland ice sheet and the eastern tethys seaway. *Paleoceanography and Paleoclimatology*, 37(8), e2022PA004415. <https://doi.org/10.1029/2022PA004415>
- Poblete, F., Dupont-Nivet, G., Licht, A., Van Hinsbergen, D. J., Roperch, P., Mihalynuk, M., et al. (2021). Towards interactive global paleogeographic maps, new reconstructions at 60, 40 and 20 Ma. *Earth-Science Reviews*, 214, 103508. <https://doi.org/10.1016/j.earscirev.2021.103508>
- Pritchard, H. D., Fretwell, P. T., Fremand, A. C., Bodart, J. A., Kirkham, J. D., Aitken, A., et al. (2025). Bedmap3 updated ice bed, surface and thickness gridded datasets for Antarctica. *Scientific Data*, 12(1), 414. <https://doi.org/10.1038/s41597-025-04672-y>
- Ramírez, D. A., Foster, D. A., Min, K., Montes, C., Cardona, A., & Sadove, G. (2016). Exhumation of the Panama basement complex and basins: Implications for the closure of the Central American seaway. *Geochemistry, Geophysics, Geosystems*, 17(5), 1758–1777. <https://doi.org/10.1002/2016GC006289>
- Sarkar, S., Basak, C., Frank, M., Berndt, C., Huuse, M., Badhani, S., & Bialas, J. (2019). Late Eocene onset of the Proto-Antarctic circumpolar current. *Scientific Reports*, 9(1), 10125. <https://doi.org/10.1038/s41598-019-46253-1>
- Scher, H. D., & Martin, E. E. (2006). Timing and climatic consequences of the opening of Drake Passage. *Science*, 312(5772), 428–430. <https://doi.org/10.1126/science.1120044>
- Schneider, B., & Schmittner, A. (2006). Simulating the impact of the Panamanian seaway closure on ocean circulation, marine productivity and nutrient cycling. *Earth and Planetary Science Letters*, 246(3), 367–380. <https://doi.org/10.1016/j.epsl.2006.04.028>
- Scotese, C. R., & Wright, N. (2018). PALEOMAP paleodigital elevation models (PaleoDEMS) for the Phanerozoic. *Paleomap Proj.*
- Sepulchre, P., Arsouze, T., Donnadieu, Y., Dutay, J. C., Jaramillo, C., Le Bras, J., et al. (2014). Consequences of shoaling of the Central American seaway determined from modeling Nd isotopes. *Paleoceanography*, 29(3), 176–189. <https://doi.org/10.1002/2013pa002501>
- Stärz, M., Jokat, W., Knorr, G., & Lohmann, G. (2017). Threshold in North Atlantic–Arctic ocean circulation controlled by the subsidence of the Greenland–Scotland ridge. *Nature Communications*, 8(1), 1–13. <https://doi.org/10.1038/ncomms15681>
- Steinthorsdottir, M., Coxall, H. K., de Boer, A. M., Huber, M., Barbolini, N., Bradshaw, C. D., et al. (2021). The Miocene: The future of the past. *Paleoceanography and Paleoclimatology*, 36(4), e2020PA004037. <https://doi.org/10.1029/2020PA004037>
- Stommel, H. (1948). The westward intensification of wind-driven ocean currents. *Eos, Transactions American Geophysical Union*, 29(2), 202–206.
- Straume, E. O., Gaina, C., Medvedev, S., & Nisancioglu, K. H. (2020). Global Cenozoic paleobathymetry with a focus on the northern hemisphere Oceanic gateways. *Gondwana Research*, 86, 126–143. <https://doi.org/10.1016/j.gr.2020.05.011>
- Sun, J., Sheykh, M., Ahmadi, N., Cao, M., Zhang, Z., Tian, S., et al. (2021). Permanent closure of the Tethyan Seaway in the northwestern Iranian Plateau driven by cyclic sea-level fluctuations in the late middle Miocene. *Palaeogeography, Palaeoclimatology, Palaeoecology*, 564, 110172. <https://doi.org/10.1016/j.palaeo.2020.110172>
- Sverdrup, H. U. (1947). Wind-driven currents in a baroclinic ocean; with application to the equatorial currents of the Eastern Pacific. *Proceedings of the National Academy of Sciences*, 33(11), 318–326. <https://doi.org/10.1073/pnas.33.11.318>
- Talley, L. D. (2003). Shallow, intermediate, and deep overturning components of the global heat budget. *Journal of Physical Oceanography*, 33(3), 530–560. [https://doi.org/10.1175/1520-0485\(2003\)033<0530:SIADOC>2.0.CO;2](https://doi.org/10.1175/1520-0485(2003)033<0530:SIADOC>2.0.CO;2)
- Thomas, M. D., De Boer, A. M., Johnson, H. L., & Stevens, D. P. (2014). Spatial and temporal scales of Sverdrup balance. *Journal of Physical Oceanography*, 44(10), 2644–2660. <https://doi.org/10.1175/jpo-d-13-0192.1>
- Toumoulin, A., Donnadieu, Y., Ladant, J.-B., Batenburg, S. J., Poblete, F., & Dupont-Nivet, G. (2020). Quantifying the effect of the Drake Passage opening on the Eocene ocean. *Paleoceanography and Paleoclimatology*, 35(8), e2020PA003889. <https://doi.org/10.1029/2020PA003889>
- Toyos, M. H., Lamy, F., Lange, C. B., Lembke-Jene, L., Saavedra-Pellitero, M., Esper, O., & Arz, H. W. (2020). Antarctic circumpolar current dynamics at the Pacific entrance to the Drake Passage over the past 1.3 million years. *Paleoceanography and Paleoclimatology*, 35(7), e2019PA003773. <https://doi.org/10.1029/2019PA003773>
- Uenzelmann-Neben, G., & Gruetzner, J. (2018). Chronology of Greenland Scotland ridge overflow: What do we really know? *Marine Geology*, 406, 109–118. <https://doi.org/10.1016/j.margeo.2018.09.008>
- van de Lagemaat, S. H. A., Swart, M. L. A., Vaes, B., Kusters, M. E., Boschman, L. M., Burton-Johnson, A., et al. (2021). Subduction initiation in the Scotia Sea region and opening of the Drake Passage: When and why? *Earth-Science Reviews*, 215, 103551. <https://doi.org/10.1016/j.earscirev.2021.103551>
- von der Heydt, A., & Dijkstra, H. A. (2005). Flow reorganizations in the Panama Seaway: A cause for the demise of Miocene corals? *Geophysical Research Letters*, 32(2). <https://doi.org/10.1029/2004gl020990>
- von der Heydt, A., & Dijkstra, H. A. (2006). Effect of ocean gateways on the global ocean circulation in the late Oligocene and early Miocene: Oligocene/miocene ocean circulation. *Paleoceanography*, 21(1). <https://doi.org/10.1029/2005PA001149>
- Westerhold, T., Marwan, N., Drury, A. J., Liebrand, D., Agnini, C., Anagnostou, E., et al. (2020). An astronomically dated record of Earth’s climate and its predictability over the last 66 million years. *Science*, 369(6509), 1383–1387. <https://doi.org/10.1126/science.aba6853>
- Xing, Q., Munday, D., Klocker, A., Sauermilch, I., & Whittaker, J. (2022). The sensitivity of the Eocene–Oligocene Southern Ocean to the strength and position of wind stress. *Climate of the Past*, 18(12), 2669–2693. <https://doi.org/10.5194/cp-18-2669-2022>
- Yang, H., Lohmann, G., Krebs-Kanzow, U., Ionita, M., Shi, X., Sidorenko, D., et al. (2020). Poleward shift of the major ocean gyres detected in a warming climate. *Geophysical Research Letters*, 47(5), e2019GL085868. <https://doi.org/10.1029/2019GL085868>

- Zhang, X., Prange, M., Steph, S., Butzin, M., Krebs, U., Lunt, D. J., et al. (2012). Changes in equatorial Pacific thermocline depth in response to Panamanian seaway closure: Insights from a multi-model study. *Earth and Planetary Science Letters*, *317*, 76–84. <https://doi.org/10.1016/j.epsl.2011.11.028>
- Zhang, Y., de Boer, A. M., Qin, G., Lunt, D. J., Hutchinson, D. K., Steinig, S., et al. (2025). Poleward expansion of North Pacific gyre circulation during the warm early Eocene inferred from inter-model comparisons. *Palaeogeography, Palaeoclimatology, Palaeoecology*, *661*, 112712. <https://doi.org/10.1016/j.palaeo.2024.112712>
- Zhang, Y., Huck, T., Lique, C., Donnadieu, Y., Ladant, J. B., Rabineau, M., & Aslanian, D. (2020). Early Eocene vigorous ocean overturning and its contribution to a warm Southern Ocean. *Climate of the Past*, *16*(4), 1263–1283. <https://doi.org/10.5194/cp-16-1263-2020>
- Zhang, Z., Nisancioglu, K. H., Flatøy, F., Bentsen, M., Bethke, I., & Wang, H. (2011). Tropical seaways played a more important role than high latitude seaways in Cenozoic cooling. *Climate of the Past*, *7*(3), 801–813. <https://doi.org/10.5194/cp-7-801-2011>

References From the Supporting Information

- Vallis, G. (2006). *Atmospheric and Oceanic fluid dynamics: Fundamentals and large-scale circulation*. Cambridge: Cambridge University Press745.